AECL EACL

CA0000138

AECL-11717, COG-96-565-I

The Effect of Geosphere Conditions on the Lifetimes of Copper Containers

L'effet des conditions de la géosphère sur la durée de vie des conteneurs en cuivre

Fraser King, Miroslav Kolář

December 1997 decembre

AECL EACL

THE EFFECT OF GEOSPHERE CONDITIONS ON THE LIFETIMES OF COPPER CONTAINERS

by

Fraser King and Miroslav Kolář

Whiteshell Laboratories
Pinawa, Manitoba, Canada R0E 1L0
1997

AECL-11717
COG-96-565-I

AECL EACL

THE EFFECT OF GEOSPHERE CONDITIONS ON THE LIFETIMES OF COPPER CONTAINERS

by

Fraser King and Miroslav Kolář

ABSTRACT

The effects of variations in geosphere conditions and of the properties of the backfill material on the performance of the engineered barriers have been examined using a numerical Cu container failure model. The thickness of the exclusion zone between the vault and the nearest major water-bearing fracture has been varied between 1 and 50 m. The groundwater [O_2] has been varied between limits of 1 and 7360 $ng \cdot g^{-1}$, the latter value being equivalent to the hypothetical situation of aerated saline groundwater at the ambient rock temperature of 17°C. The properties of the excavation-disturbed zone (EDZ) have been varied to simulate both blast-induced and stress-induced damage. Finally, the effect of the particle size of crushed granite, of reduced heat output from the container and the effect of substituting pyrite for biotite on the performance of the backfill material has been determined. The impact of these variables on the corrosion rate, the extent of the four O_2-consumption reactions and the fate of Fe(II) dissolved from the biotite (or pyrite) in the backfill and EDZ has been examined.

The results of the various simulations suggest that the engineered barriers (the container and the buffer and backfill materials) can isolate the fuel almost indefinitely, regardless of the geosphere conditions. Copper containers are predicted not to fail by corrosion within the analysis period of ~10^5 a. The robustness of the engineered barriers is a result of (i) the low rates of mass transport in saturated buffer and backfill materials and (ii) the presence of an excess of redox-buffering Fe(II) minerals in the backfill.

Whiteshell Laboratories
Pinawa, Manitoba, Canada R0E 1L0
1997

AECL-11717
COG-96-565-I

AECL EACL

L'EFFET DES CONDITIONS DE LA GÉOSPHÈRE SUR LA DURÉE DE VIE DES CONTENEURS EN CUIVRE

par

Fraser King et Miroslav Kolář

RÉSUMÉ

Les effets de variations des conditions de la géosphère et des propriétés du matériau de remblayage sur le comportement des barrières artificielles ont été examinés en utilisant un modèle de défaillance numérique du conteneur en Cu. On a fait varier l'épaisseur de la zone d'exclusion entre l'enceinte et la fracture de l'aquifère principale la plus près entre 1 et 50 m. On a fait varier les eaux souterraines [O_2] entre les limites de 1 et 7 360 $ng \cdot g^{-1}$, cette dernière valeur étant équivalente à la situation hypothétique d'eaux souterraines salines aérées à la température ambiante de la roche de 17 °C. On a fait varier les propriétés de la zone perturbée par l'excavation pour simuler les dommages dus au dynamitage et aux contraintes. Finalement, on a déterminé l'effet de la granulométrie du granite concassé, de la production de chaleur réduite provenant du conteneur et l'effet du remplacement de la biotite par la pyrite sur le comportement du matériau de remblayage. On a également examiné les conséquences de ces variables sur la vitesse de corrosion, sur l'ampleur des quatre réactions de consommation d'O_2 et sur le sort du Fe (II) dissous provenant de la biotite (ou de la pyrite) dans le remblai et la zone perturbée par l'excavation.

Les résultats de ces diverses simulations indiquent que les barrières artificielles (le conteneur et les matériaux tampon et du remblayage) peuvent isoler presque indéfiniment le combustible, quelles que soient les conditions de la géosphère. On ne prévoit pas de défaillance des conteneurs en cuivre due à la corrosion dans la période d'analyse de ~10^5 a. La robustesse des barrières artificielles résulte (i) des faibles vitesses de transport de masse dans les matériaux tampon et de remblayage et (ii) de la présence d'un excès de minéraux de Fe(II) à pouvoir tampon d'oxydoréduction dans le remblai.

Laboratoires de Whiteshell
Pinawa (Manitoba) Canada R0E 1L0
1997

AECL-11717
COG-96-565-I

CONTENTS

1. INTRODUCTION

The geosphere is one of the natural and engineered barriers in the multi-barrier system currently being assessed for the disposal of nuclear fuel waste in Canada (AECL 1994). These barriers, which include the 500-1000 m of granitic rock of the geosphere and the container, buffer and backfill materials in the vault, act as a total system. Over the past several years, however, increasing evidence has suggested that very long container lifetimes (in excess of 10^6 a) may be achievable using oxygen-free Cu or crevice-corrosion resistant Ti alloys (Shoesmith et al. 1995). If this were the case, less reliance may need to be placed on the geosphere as a barrier, since the vast majority of radionuclides would decay before being released from the vault (Johnson et al. 1996).

Chemical and mass-transport conditions in the vault are influenced by the presence and the properties of the host rock. Consequently, the nature of the geosphere influences the corrosion behaviour of the containers in a number of ways. First, in highly fractured rock, advective mass transport may occur in the vault sealing materials as well as diffusion, particularly in the backfill. Second, water/rock interactions in the geosphere determine the chemistry of the groundwater. In particular, deep groundwaters in the Canadian Shield tend to be O_2-free and saline (Frape et al. 1984, Gascoyne et al. 1996). Third, the thermal properties of the rock affect the temperature profiles within the vault. Finally, deep sub-surface environments are much less supportive of microbial activity than near-surface environments.

The greatest influence of the geosphere on the corrosion behaviour of both Cu and Ti containers is the low dissolved $[O_2]$ in deep groundwaters (≤ 1 ng·g^{-1}, Gascoyne et al. 1996). Because the groundwater is an insignificant source of oxidant, the environment within the disposal vault is expected to evolve from oxidizing to non-oxidizing as the O_2 initially trapped in the pores of the buffer and backfill materials is consumed by corrosion and other processes and is not replenished (Kolář and King 1996). For Cu, corrosion is predicted to cease once all the oxidant in the vault (present either as O_2 or as Cu(II) species produced by the homogeneous oxidation of Cu(I) by O_2) is exhausted (King and Kolář 1995, 1996).

Of secondary importance in the corrosion behaviour of Cu is the salinity of the groundwater. Although Cl^- ions play an important role in the speciation of dissolved Cu, their concentration affects neither the rate nor the extent of corrosion. Increased temperature or rate of mass transport in the vault could lead to higher corrosion rates, but, provided no extra oxidant enters the vault, higher corrosion rates will only shorten the period before corrosion stops.

An assessment of the corrosion behaviour of containers for a study of in-room disposal (Johnson et al. 1996) resulted in lifetimes in excess of 10^6 a for 25-mm-thick Cu containers (King 1996). Two forms of corrosion were considered, uniform corrosion and pitting. For this assessment, the rock barrier was relatively permeable, its main function being to maintain a dissolved $[O_2]$ of 5 ng·g^{-1}. In the calculation of the rate of uniform

corrosion (King 1996), the $[O_2]$ was assumed to be maintained at 5 $ng \cdot g^{-1}$ at the excavation-disturbed zone (EDZ)/sparsely fractured rock interface. Furthermore, all dissolved Cu corrosion products diffusing out of the vault were assumed to be swept away at this boundary. Therefore, no credit was taken for the mass-transfer resistance offered by the 500-1000-m-thick layer of rock (King 1996).

In this report, the dependence of the rate of uniform corrosion of copper containers on the properties of the rock is determined for a number of different scenarios. Since the maximum container pit depth of 6 mm is assumed to be independent of the geosphere conditions, these calculations also give the container lifetimes. First, the dependence of the container lifetime on the distance between the EDZ and the nearest major fracture (i.e., the exclusion distance) is examined for a fixed groundwater $[O_2]$. Second, the effect of various $[O_2]$ on the container lifetime is determined. Third, the effects of the properties of the EDZ on the rate of uniform corrosion are examined and, finally, the impact of changes in the composition of the backfill material on its ability to act as a redox barrier are reported.

2. SCENARIOS CONSIDERED

2.1 UNIFORM CORROSION MODELS

The uniform corrosion model for Cu containers involves a numerical solution of a number of coupled reaction-diffusion equations in a 1-dimensional multi-layer medium (Kolář and King 1997). The four layers considered in the current version of the model are the buffer and backfill materials, the EDZ and the layer of sparsely fractured rock between the EDZ and the nearest major water-bearing fracture (Figure 1). The thickness of these layers can be adjusted to simulate the effect of different vault designs, EDZ properties and rock conditions.

The reaction-diffusion equations are based on the reaction mechanism shown in Figure 2. Mass-balance equations of the general type

$$\varepsilon_a \frac{\partial c}{\partial t} = \frac{\partial}{\partial x}\left(\varepsilon_e \tau D_0 \frac{\partial c}{\partial x}\right) + \varepsilon_a \sum_i R_i + \sum_i R_i' \qquad (1)$$

are written for each of the 10 chemical species included in the model, where c is the pore-water concentration, ε_a and ε_e are the accessible and effective porosities, τ is the tortuosity factor, D_0 the bulk solution diffusion coefficient and $\sum_i R_i$ and $\sum_i R_i'$ are reaction terms for dissolved and precipitated (or adsorbed) species, respectively, summed over all possible reactions i (King and Kolář 1995, King et al. 1996). The ten chemical species included in the model are dissolved O_2, O_2 in the vapour phase, $CuCl_2^-$, Cu_2O, Cu^{2+}, $CuCl_2 \cdot 3Cu(OH)_2$, adsorbed Cu^{2+}, Cl^-, dissolved Fe(II) and precipitated Fe(II). In addition, a heat-conduction equation is included, because all of the diffusion coefficients

and rate parameters are temperature dependent. Consequently, the value of these parameters varies spatially and temporally within the vault as the temperature changes. More detailed descriptions of the model are given by King and Kolář (1995, 1996) and Kolář and King (1997).

Two versions of the uniform corrosion model for Cu are used in the present calculations. In both cases, the heat conduction equation is solved for all four layers, i.e., the thermal properties of the buffer, backfill, EDZ and rock layer are used to calculate the temperature profiles within the vault. The difference between the two models is in the treatment of mass transfer in the rock layer. In the full version of the model, named "centrH" for central case with Heat, the boundary for the mass-transport calculations is placed at the right-hand side of the rock layer (Figure 1). Thus, for centrH, the properties of all four layers are used for both heat and mass-transfer calculations. In the other version of the model, named "centrHnr" for central case with Heat but no rock, the boundary for the mass-transport calculations is at the EDZ/rock interface.

The codes contain a number of control parameters that can be used to vary the accuracy or execution time of the calculations. In general, the higher the desired accuracy, the longer the execution time. In the interests of performing a large number of calculations, the runs reported here were carried out at a lower accuracy. Comparison of the results with more accurate runs suggests that the maximum possible error is of the order of 10%.

2.2 COMMON ASSUMPTIONS

There are a number of common assumptions for the various scenarios considered here (Table 1). The basis for, and consequences of, these various assumptions are discussed in Section 4.

2.3 VARIATION IN EXCLUSION-ZONE THICKNESS

A waste exclusion zone separates the edge of the vault, taken here as the edge of the EDZ, from the nearest major fracture, along which transport to the surface is assumed to be relatively fast. Mass transport through this rock layer would be expected to be slow as a result of the low porosity and high tortuosity of the sparsely fractured rock found at depth at the Underground Research Laboratory (URL) site. In the reference vault design for the Environmental Impact Study (EIS) (AECL 1994), an exclusion-zone thickness of 50 m was assumed. Diffusion was the dominant mass-transport mechanism within this exclusion zone. The 50-m-thick layer of low-permeability rock was found to be a more effective barrier than either the Ti container or buffer and backfill materials (AECL 1994).

In the recent performance assessment of the in-room disposal of copper containers in permeable rock (Wikjord et al. 1996), less significance was placed on the rock as a mass-transport barrier. Although the exclusion distance was maintained at 50 m, the permeability of the rock was increased by two orders of magnitude. Consequently,

advection was the dominant mass-transport mechanism and the rock layer became a relatively insignificant barrier.

The thickness of the exclusion zone depends on the quality of the rock in which the vault is located. In the event that a suitable site with a sufficiently large body of sparsely fractured rock cannot be found in the Canadian Shield, it may become necessary to accept a smaller exclusion zone than that assumed in the EIS. In addition, it is useful to examine the effect of the exclusion-zone thickness to counter arguments that the minimum thickness of 50 m stipulated in the EIS cannot be guaranteed.

Here, we examine the impact of various exclusion-zone thicknesses on the lifetimes of copper containers. The thickness of the layer of sparsely fractured rock (Figure 1) was defined as either 1, 5, 10 or 50 m, with an effective porosity and tortuosity factor of 0.004 and 0.0587, respectively. The groundwater [O_2] was 1 ng·g^{-1}. The centrH version of the model was used. Since the ambient rock temperature of 17°C is defined at the rock/fracture interface, the calculated temperature profiles vary with the thickness of the layer of sparsely fractured rock. Consequently, the maximum container skin temperature and temperature profiles within the vault vary slightly from run to run.

2.4 GROUNDWATER OXYGEN CONCENTRATION

Oxygen is expected to be the major oxidizing species in the disposal vault (Kolář and King 1996). Deep Canadian Shield groundwaters typically contain <1 ng·g^{-1} dissolved O_2 (Gascoyne et al. 1996) and, consequently, are expected to be an insignificant source of oxidant for container corrosion (Kolář and King 1996).

Despite the fact that O_2 in the groundwater is unlikely to contribute to the corrosion of the container, it is of interest to examine to what extent the vault design can compensate for elevated [O_2] in the groundwater. Diffusion of O_2 into the vault will be limited by the low-permeability buffer and backfill materials. Furthermore, the backfill contains a significant quantity of Fe(II) minerals, in the form of crushed biotite-containing granite, which will act as a redox barrier against the transport of O_2 to the container surface.

In the present analyses, groundwater [O_2] of 1, 5, 10, 30, 100, 300, 1000, 3000 and 7360 ng·g^{-1} have been assumed (the latter concentration is equivalent to air-saturated saline, Na-/Ca-based groundwater with a [Cl^-] of ~1.0 mol·dm^{-3} at a temperature of 17°C, Battino et al. 1983). There is no geological basis for choosing these values since there is no evidence that actual [O_2] deep underground in the Canadian Shield will exceed 1 ng·g^{-1}. These [O_2] values have simply been chosen to investigate the robustness of the engineered barriers.

The calculations were performed with the centrHnr version of the model. Consequently, the various [O_2] defined above were imposed at the EDZ/rock interface, with no consumption of O_2 in the layer of sparsely fractured rock. The full thickness of 50 m of rock is used for the thermal calculations.

2.5 PROPERTIES OF EXCAVATION-DISTURBED ZONE

The three parameters in the model that are used to simulate transport in the EDZ are the length (L), porosity (ε) and tortuosity factor (τ). Mass transport occurs by diffusion only. A steady-state mass-transfer coefficient (k_M) can be defined

$$k_M = \varepsilon\tau D_0/L \qquad (2)$$

where D_0 is the diffusion coefficient in bulk solution.

In engineering studies, the hydraulic conductivity is often used to characterize the EDZ (Chandler et al. 1996). Unfractured rock at the Underground Research Laboratory (URL) has a low hydraulic conductivity ($< 10^{-13}$ m·s^{-1}), and transport is primarily by diffusion. At higher conductivities, advection becomes increasingly important.

Two types of EDZ have been characterized at the URL (Chandler et al. 1996). If the vault is excavated using a drill-and-blast technique, an EDZ perhaps 5-10-cm thick will be created, but will not be continuous along the length of the tunnel. The hydraulic conductivity of the blast-induced EDZ may be of the order of 10^{-10}-10^{-12} m·s^{-1} (Chandler et al. 1996), up to three orders of magnitude higher than the unfractured rock. Damage can also be induced by rock stresses. For highly stressed rock, "notching" can occur in the roof and floor of the disposal rooms. This notching can result in a 15-30-cm-thick EDZ connected along the length of the room, with a hydraulic conductivity of 10^{-7}-10^{-8} m·s^{-1} (Chandler et al. 1996).

In the copper corrosion model, the reference EDZ is assumed to be 10-cm thick with a porosity of 0.008 and a tortuosity factor of 0.0587, corresponding to a k_M value of 5×10^{-12} m·s^{-1}. The equivalent value of k_M for the 50-m-thick layer of sparsely fractured rock is 5×10^{-15} m·s^{-1}, the difference of three orders of magnitude being approximately equal to that observed between the hydraulic conductivities of unfractured rock and the blast-induced EDZ at the URL. Consequently, the reference EDZ properties will be assumed to simulate the presence of blast-induced damage. To simulate the stress-induced EDZ properties, a thickness of 30 cm was used and the porosity and tortuosity factor increased to give a k_M value of 2×10^{-9} m·s^{-1}.

The centrHnr version of the model was used for the simulations with a groundwater [O_2] of 1 ng·g^{-1}.

2.6 BACKFILL MATERIAL COMPOSITION AND PROPERTIES

As stated above, the properties of the backfill material can offset the effects of increasing [O_2] in the groundwater. The reference upper (or dense) backfill composition in the EIS case study (AECL 1994) and the in-room case study (Johnson et al. 1996) consists of 70 wt.% crushed granite. Granite from the URL excavations contains ~5 wt.% biotite

(J. Cramer, private communication, 1995), having the general formula $K(Mg_{0.6\text{-}1.8}Fe^{II}_{2.4\text{-}1.2})(Si_3Al)O_{10}(OH, F)_2$. Dissolution (alteration) of biotite leads to the release of Fe(II), which can then undergo oxidation to Fe(III) or precipitation as an Fe(II) solid (Malmstrom et al. 1995; Taylor and Owen 1995, 1997). In addition, exposed fracture surfaces in the EDZ and sparsely fractured rock will also contain biotite which will react with O_2 in the groundwater. The reference buffer material contains relatively little Fe(II), although, along with the backfill, it does contain oxidizable organic material that will also consume O_2 in the vault (Kolář and King 1996).

The Fe(II) dissolution and oxidation reactions are treated in the model using the following equations

$$Fe(II)_{biotite} \rightarrow Fe(II)_{aq} \tag{3}$$

$$4Fe(II)_{aq} + O_2 + 2H_2O \rightarrow 4Fe(III)_{aq} + 4OH^- \tag{4}$$

$$Fe(III)_{aq} \rightarrow Fe(III)_{ppt} \tag{5}$$

$$Fe(II)_{aq} \leftrightarrow Fe(II)_{ppt} \tag{6}$$

$$Fe(II)_{aq} + Cu^{2+} + 2Cl^- \rightarrow Fe(III)_{aq} + CuCl_2^- \tag{7}$$

Thus, $Fe(II)_{aq}$ can be oxidized by both O_2 and Cu^{2+}. Furthermore, any $Fe(II)_{aq}$ not oxidized is assumed to precipitate once the $[Fe(II)_{aq}]$ exceeds the solubility (taken to be 10^{-5} mol·dm^{-3}). This precipitation process is assumed to be reversible, so that dissolved and precipitated Fe(II) can accumulate in the system, acting as a redox barrier to the ingress of O_2 from the groundwater and the egress of Cu(II) or oxidized radionuclides from the vault.

The kinetics of the dissolution step (Reaction (3)) are given by

$$d[Fe(II)_{aq}]/dt = A_F[R_0e^{-\alpha t} + R_1] \tag{8}$$

where A_F is the surface area of exposed biotite (or other Fe(II)-containing mineral), R_0 and R_1 are the instantaneous and steady-state dissolution rates and α is a time constant. This kinetic expression is consistent with the experimental observation that the dissolution rate decreases with time as a layer enriched in the least soluble species builds up on the biotite surface (Malmstrom et al. 1995). Experimentally, steady state is achieved after 6-12 months, so that for the timescales of interest here we are primarily concerned with the steady-state dissolution kinetics. Each of the rate parameters in Equation (8) (R_0, R_1 and α) are assumed to be temperature dependent and obey Arrhenius-type relationships, e.g.,

$$\log [R_1(T_1)/R_1(T_2)] = -2.3\Delta E/R[(T_2-T_1)/T_1T_2] \tag{9}$$

where $R_1(T_1)$ and $R_2(T_2)$ are the values of R_1 at temperatures T_1 and T_2 and ΔE and R are the activation energy and gas constant, respectively.

The ability of the backfill to act as a redox barrier can be examined in a number of ways. First, the effective surface area of exposed biotite can be varied to simulate different distributions of particle size of the graded crushed granite. The estimated exposed surface area of biotite for the reference backfill material is 7.89 dm^{-1} (A_F is expressed as the exposed area per unit volume of backfill material, Appendix A). If a smaller range of particles sizes is used (< 0.2 cm), A_F is increased to 15.7 dm^{-1}. For the in-room disposal concept, granitic sand is used in a 1:1 mixture with Na-bentonite in the light backfill (Johnson et al. 1996). The exposed surface area of biotite in the light backfill is estimated to be 88.5 dm^{-1} (Appendix A). Second, the dependence of the dissolution rate of biotite on temperature can be examined by changing the heat output of the container (H_0). Here, H_0 has been reduced by a factor of 2 to simulate the effect of fuel that is cooled longer than the 10-year period assumed in the EIS. Third, the effect of substituting (or adding) a different O_2 scavenger can be simulated by changing the values of R_0, R_1, α_F and their respective activation energies. Pyrite is known to oxidize more rapidly than biotite (Werme et al. 1992), and the effect of substituting pyrite for biotite in the backfill material is simulated here by simply increasing the steady-state dissolution rate (R_1) by the appropriate amount.

The centrHnr version of the model was used for the simulations with a groundwater [O_2] of 5 $ng \cdot g^{-1}$.

3. RESULTS OF SIMULATIONS

In all the simulations discussed below, the initial quantity of O_2 in the vault and the maximum inventory of Fe(II) in the backfill material are constant. Many of the results presented below will be discussed in terms of the fate of the initially trapped O_2 and the Fe(II) released from the biotite.

For the vault dimensions used here, the amount of O_2 initially trapped in the buffer and dense backfill materials is 0.0111 $mol \cdot dm^{-2}$, of which 0.00866 $mol \cdot dm^{-2}$ or 78% is in the buffer (because of the 1-dimensional nature of the model, many parameters are expressed per unit cross-sectional area). This O_2 is consumed in four processes: (i) electrochemical reduction on the container surface causing corrosion, (ii) diffusion out of the vault, (iii) oxidation of $CuCl_2^-$ and (iv) oxidation of $Fe(II)_{aq}$.

The maximum amount of available Fe(II) in the dense backfill is 2.6 $mol \cdot dm^{-2}$ (Kolář and King 1997), representing a ~60-fold excess over the amount of trapped O_2 (1 mol O_2 reacts with 4 mol Fe(II), Reaction (4)). (The amount of Fe depends on the stoichiometry assumed for biotite. The value of 2.6 $mol \cdot dm^{-2}$ is based on $K_2Fe_2MgAl_2Si_6O_{20}(OH)_4$). In addition, the EDZ contains a further 0.4 $mol \cdot dm^{-2}$ Fe(II) on the exposed fracture surfaces (Kolář and King 1997). Once dissolved from the biotite (or pyrite) matrix, dissolved

$Fe(II)_{aq}$ will either (i) react with dissolved O_2 (Reaction (4)), (ii) react with Cu(II) (Reaction (7), or (iii) accumulate in the system as dissolved or precipitated Fe(II) (Reaction (6)).

3.1 EFFECT OF EXCLUSION-ZONE THICKNESS

Table 2 gives the results of simulations performed with centrH with various exclusion-zone thickness for a total period of 10^5 a. Because the rock-layer thickness is used in the thermal calculations, the temperature profiles within the vault vary with the assumed exclusion-zone thickness. An indication of the significance of this effect is given in Table 2 in terms of the maximum container-surface temperature and the time at which that maximum temperature is attained. Smaller exclusion-zone thicknesses lead to greater heat loss from the vault, resulting in lower maximum surface temperatures attained at shorter times.

The data in Table 2 indicate that there is no effect of the exclusion-zone thickness on the extent of corrosion of the container. The mean value of the integrated corrosion current density $\int i_{CORR}$ (3700 ± 300 C·dm^{-2}) corresponds to a wall penetration of 27 μm. Of this total corrosion, only ~1% is caused by the interfacial reduction of O_2 ($\int i_{O2}$), the vast majority being caused by the reduction of Cu^{2+}. Thus, reducing the exclusion-zone thickness does not lead to higher corrosion rates because of the diffusion of O_2 into the vault from the groundwater. In fact, for these O_2-deficient groundwaters ($[O_2]$ = 1 ng·g^{-1} in this case), reducing the exclusion-zone thickness tends to lead to a greater flux of O_2 out of the vault.

The vast majority (> 70%) of the O_2 initially trapped in the vault is predicted to be consumed by the oxidation of $CuCl_2^-$ to Cu^{2+}. (The amounts of O_2 consumed by corrosion, diffusion out of the vault and the two oxidation reactions do not add up to the initial inventory of 0.0111 mol·dm^{-2} because of numerical integration errors. The % values given here have been normalized to give a total consumption of 100%). This reaction indirectly leads to corrosion of the container as some of this Cu^{2+} is reduced on the container surface. The next most significant O_2-consumption process is the oxidation of Fe(II), primarily in the backfill (14-29%). Since the dissolution rate of Fe(II) from biotite is highly temperature dependent (activation energy 60 kJ·mol^{-1}), the extent of Fe(II) oxidation is predicted to increase with exclusion-zone thickness because of the increase in vault temperature. This effect, however, is largely an artifact of the construction of the model, since the ambient rock temperature of 17°C is imposed at the right-hand side of the rock layer (Figure 1). In reality, the temperature profiles within the vault are likely to be less sensitive to the distance between the vault and the nearest major fracture, so that the extent of O_2 consumption by biotite oxidation will be less dependent on the exclusion-zone thickness.

The effect of the variation in temperature within the vault can also be seen in the amount of Fe(II) predicted to accumulate in the system. Because the dissolution rate increases

with temperature, the amounts of both $Fe(II)_{aq}$ and $Fe(II)_{ppt}$ increase with exclusion-zone thickness. In all cases, however, a significant amount of Fe(II) remains unreacted after dissolving from the biotite. Thus, the backfill acts as a significant redox barrier and not only consumes much of the O_2 in the vault but also reduces all Cu^{2+} to $CuCl_2^-$. (The predicted amount of $Fe(II)_{ppt}$ is ten times the amount of $Fe(II)_{aq}$ because the rate constant for Fe(II) precipitation is ten times that for the dissolution step and both are sufficiently fast that equilibrium is effectively established in the backfill).

3.2 EFFECT OF GROUNDWATER OXYGEN CONCENTRATION

A number of simulations were performed with the model centrHnr using different groundwater $[O_2]$, up to a maximum time period of 10^5 a. Some of the results are summarized in Table 3. In the centrHnr code, the groundwater $[O_2]$ is imposed as a boundary condition at the EDZ/rock interface. Consequently, the geosphere does not act as a barrier to the mass transport of species in or out of the vault. For thermal calculations, however, the assumed 50-m exclusion zone is included. Figure 3 shows the predicted variation of the container surface temperature with time and the temperature profiles in the vault and rock for various intervals following vault closure. The container surface temperature profile is similar to that predicted for containers near the centre of the disposal vault using more detailed thermal calculations that take into account the effects of neighbouring containers (Baumgartner et al. 1995).

From the data in Table 3, it can be seen that the groundwater $[O_2]$ has no effect on the predicted extent of corrosion of the container. The mean integrated corrosion current density of 4000 ± 800 C·dm^{-2} is equivalent to a wall penetration of 29 ± 6 μm. The reason that the groundwater $[O_2]$ has no effect on the corrosion rate is the large redox capacity of the backfill which prevents O_2 from the groundwater from reaching the container. Corrosion of the container is primarily caused by the O_2 trapped initially in the buffer. For these simulations, there is assumed to be no O_2-scavenging species in the buffer. (In fact, it is believed that the microbially mediated oxidation of organic matter may consume most of the O_2 in the buffer (Kolář and King 1996)). The O_2 in the buffer is either directly reduced on the container surface, or oxidizes dissolved $CuCl_2^-$ to Cu^{2+}, which then acts as the oxidant. This redox cycle is autocatalytic, since the reduction of one Cu^{2+} species leads to the formation of two $CuCl_2^-$ ions, which can then be reoxidized to two more Cu^{2+} species

$$CuCl_2^- + \tfrac{1}{4}O_2 + \tfrac{1}{2}H_2O \rightarrow Cu^{2+} + 2Cl^- + OH^- \quad (10)$$

$$Cu^{2+} + Cu + 4Cl^- \rightarrow 2CuCl_2^- \quad (11)$$

$$2CuCl_2^- + \tfrac{1}{2}O_2 + H_2O \rightarrow 2Cu^{2+} + 4Cl^- + 2OH^- \quad (12)$$

This catalytic cycle continues at an increasing rate until the O_2 in the vault becomes exhausted. Since the rates of the homogeneous oxidation of $CuCl_2^-$ by O_2 and of the

interfacial reduction of Cu^{2+} exceed that of the interfacial reduction of O_2, the majority of the corrosion (~99%) is caused by the reduction of Cu^{2+}.

The data in Table 3 also suggest that there is relatively little effect of the groundwater $[O_2]$ on the performance of the vault as a whole for $[O_2] < 300$ ng·g^{-1}. Column 7 of Table 3 gives the ratio of the sum of the four O_2-consumption reactions (listed individually in columns 3-6) to the quantity of O_2 trapped initially in the buffer and backfill materials (0.0111 mol·dm^{-2}). For $[O_2] < 300$ ng·g^{-1}, the value of this ratio is ~1 (values < 1 are a result of the integration errors in the code). Figure 4 illustrates the variation of the integrated values of the four O_2-consumption reactions as a function of groundwater $[O_2]$ for a simulation time of 10^5 a.

At all groundwater $[O_2]$, O_2 diffuses out of the vault and is swept away by the flowing groundwater assumed to exist at the EDZ/rock boundary. This is a consequence of the higher $[O_2]$ in the vault initially. Even over a period of 10^5 a, little O_2 diffuses back into the buffer and backfill materials because of the low permeability of the EDZ.

For groundwater $[O_2] > 300$ ng·g^{-1} (> 9.38 x 10^{-6} mol·dm^{-3}), an increase in the extent of $CuCl_2^-$ and Fe(II) oxidation is predicted to occur. In aerated groundwater, the extent of $CuCl_2^-$ oxidation is ~5 times higher than for a groundwater $[O_2]$ of 1 ng·g^{-1}, whilst the extent of Fe(II) oxidation increases by a factor of ~8 for the same conditions. Since the groundwater is the source of O_2, these oxidation reactions occur primarily in the backfill material and EDZ. Thus, O_2 is consumed by reaction with Fe(II) prior to reaching the container surface. In addition, Cu^{2+} formed by the oxidation of $CuCl_2^-$ in the backfill is either reduced back to $CuCl_2^-$ or diffuses out of the vault before coming into contact with the container. Consequently, no additional corrosion is observed, either directly from the interfacial reduction of O_2 or indirectly because of Cu^{2+} produced from the homogeneous oxidation reaction.

The simulations also suggest that the redox capacity of the buffer is not exhausted within a period of 10^5 a, even in aerated groundwater, since $Fe(II)_{aq}$ and $Fe(II)_{ppt}$ accumulates in the backfill (last two columns, Table 3). In order to determine to what extent the Fe(II) minerals continue to act as a redox barrier, a simulation with aerated groundwater was extended to a period of 3.5 x 10^5 a. Figure 5 shows the time dependence of the integrated fluxes for the four O_2-consumption reactions. Corrosion supported by the reduction of O_2 ceases after ~1000 a. Oxygen that continues to enter the vault after this period only serves to oxidize $CuCl_2^-$ or Fe(II). Since, the oxidation of $CuCl_2^-$ occurs some distance from the container, it is unlikely that much additional corrosion results from the Cu^{2+} so formed. Instead, the Cu^{2+} is more likely to be reduced by reaction with Fe(II) in the backfill.

The integrated flux of O_2 at the backfill/EDZ boundary in aerated groundwater reaches a maximum after ~780 a and then decreases slightly (Figure 5). Initially O_2 is predicted to diffuse out of the vault. This is an artifact resulting from the elevated $[O_2]$ assumed initially for the buffer and backfill materials (assumption 1, Table 1). As the $[O_2]$ drops

below that in the groundwater (2.3×10^{-4} mol·dm^{-3} in this simulation), O_2 diffuses back into the vault. The decrease in the flux at the backfill/EDZ boundary (the flux out of the vault is defined as positive), however, is less than that which would be expected based on the amount of Fe(II) oxidized by O_2 in the backfill and EDZ layers (column 6, Table 3). This suggests that, in the simulation, much of the oxidation of Fe(II) occurs in the EDZ or at the backfill/EDZ boundary, and not in the backfill layer itself. This reaction occurs primarily in the EDZ because the effective diffusion coefficient of $Fe(II)_{aq}$ diffusing out of the backfill is ~6 times larger than that for O_2 diffusing in through the EDZ because of the higher porosity and tortuosity factor of the backfill. Although this would also tend to occur in an actual disposal vault, an oxidized front moving into the backfill would also be expected under these conditions, as the biotite in the EDZ becomes fully oxidized. This effect cannot be simulated in the present version of the model because the inventory of Fe(II) is assumed to be unlimited. This is a reasonable assumption for the majority of simulations, but becomes invalid in simulations with high groundwater [O_2] and extensive oxidation of Fe(II).

Figure 6 shows the fate of the Fe(II) in the backfill and EDZ layers over a period of 3.5×10^5 a in the case of aerated groundwater. The total initial inventory of Fe(II) in the backfill and EDZ amounts to 2.6 mol·dm^{-2} and 0.44 mol·dm^{-2}, respectively. This inventory is steadily consumed by reaction with O_2 throughout the simulation period. Accumulation of $Fe(II)_{aq}$ and $Fe(II)_{ppt}$ in the vault only occurs after a period of 1050 a, at which time ~93% of the initial inventory of O_2 has been consumed. At about the same time, Cu^{2+} diffuses into the backfill and is reduced by reaction with Fe(II). After 3.5×10^5 a the sum total of the fluxes for these four processes is equal to 0.68 mol·dm^{-2}, which corresponds to ~22% of the initial inventory of Fe(II) in the backfill and EDZ.

3.3 EFFECT OF EDZ PROPERTIES

Table 4 shows the results of two simulations with different EDZ properties. The centrHnr version of the model, in which the right-hand mass-transport boundary is situated at the EDZ/rock interface, was used for these runs. Both simulations were run for a period of 73510 a with a groundwater [O_2] of 1 ng·g^{-1} (3.1×10^{-8} mol·dm^{-3}). The first simulation with a steady-state diffusive mass-transfer coefficient of 5×10^{-12} m·s^{-1} represents a 10-cm-thick blast-induced layer, whilst the second run ($k_M = 2 \times 10^{-9}$ m·s^{-1}) simulates enhanced diffusion through a 30-cm-thick stress-induced EDZ.

There is little effect of this change in EDZ properties on the corrosion of the container or the performance of the vault. The higher value of $\int i_{CORR}$ for the higher permeability EDZ (6220 C·dm^{-2}, corresponding to 46 μm wall penetration) is believed to be an artifact due to numerical integration errors rather than a reflection of increased corrosion.

The major effect of the increased EDZ permeability is to permit more of the O_2 initially trapped in the vault to diffuse out. The predicted flux of O_2 at the backfill/EDZ boundary doubles when the permeability of the EDZ is increased. As a consequence, the time to consume the trapped O_2 in the vault decreases by ~270 a. Once the initial O_2 has been

consumed, however, the more permeable EDZ allows more O_2 from the groundwater into the vault. This is reflected in the greater extent of Fe(II) oxidation by O_2 (column 6, Table 4) and the smaller amounts of accumulated $Fe(II)_{aq}$ and $Fe(II)_{ppt}$. The extent of additional Fe(II) oxidation for the permeable EDZ is small, however, when compared with the total Fe(II) content of the backfill and EDZ of 3.0 $mol \cdot dm^{-2}$.

3.4 EFFECT OF BACKFILL MATERIAL PROPERTIES

The results presented in Section 3.2 clearly show that the backfill can act as a significant barrier to the ingress of O_2 from the groundwater. The effectiveness of this barrier depends on a number of factors. Obviously, the total redox buffering capacity depends on the inventory of Fe(II) minerals in the backfill. Also of importance is the rate at which Fe(II) dissolves and becomes available for reaction with O_2 and Cu^{2+}. The kinetics of Fe(II) dissolution (Equation (8)) are affected by (i) the surface area of exposed Fe(II)-containing mineral (A_F), (ii) temperature (e.g., Equation (9)), and (iii) the nature of the Fe(II) mineral.

The surface areas of exposed biotite for the reference dense backfill material, for dense backfill material comprising more finely crushed granite and for the bentonite/granitic sand light backfill material defined for the in-room disposal concept (Johnson et al. 1996) are given in Appendix A.

Table 5 shows the results of simulations for backfill material of these three compositions. As would be expected, the time to consume all the initial O_2 in the vault (defined as the time to reduce the quantity of O_2 in the buffer, backfill and EDZ to <0.01% of its original value) decreases with increasing surface area of biotite. Thus, the light backfill material containing granitic sand is a more effective O_2 scavenger than the dense backfill, which contains coarser aggregate. It should be remembered, however, that these simulations do not include the effect of organic material on O_2 consumption in the buffer and backfill.

Within the accuracy of the numerical analyses, there appears to be no significant effect on either the total amount of corrosion or the amount of corrosion supported by the interfacial reduction of O_2. The effect of more rapid biotite dissolution, therefore, is to more quickly consume O_2 in the backfill, without consuming O_2 in the buffer closest to the container.

Temperature also has a significant effect on the time to consume all the O_2 in the vault. If the heat output from the container is halved, the maximum container surface temperature drops from 81°C to 49°C (cf. Figures 3(a) and 7(b)). More importantly, the temperature in the backfill also drops. As a consequence, the rate of biotite dissolution is lower and the time for O_2 consumption increases from 1670 a to 2850 a. Since the activation energy for the steady-state dissolution rate R_1 is 59 $kJ \cdot mol^{-1}$, R_1 doubles for each 10°C increase in temperature, over the temperature range 273-373 K (Equation (9)). Comparison of the temperature profiles in the backfill (Figures 3(b) and 7(b)) for various exposure periods shows that the dissolution rate of biotite would be significantly higher for the hotter

container. The results of the simulations suggest that only 17% of the initial inventory of O_2 is consumed by reaction with biotite for the cooler container, compared with 27% for the case of the reference 10-a-cooled fuel.

Substituting pyrite for biotite also leads to more rapid O_2 consumption. The steady-state alteration rate of pyrite is ~3 orders of magnitude higher than that for biotite (Werme et al. 1992). For the same exposed mineral surface area, O_2 consumption in the vault as a whole would be complete after 510 a if pyrite were the active redox agent in the backfill compared with 1670 a for biotite (Table 5). The difference is even more dramatic in the backfill layer (Figure 8). For pyrite, the O_2 in the backfill layer is consumed within ~8 a, compared with ~1000 a for biotite. This difference is even more dramatic when it is considered that, after only 8 a, the temperature in the backfill will not have increased significantly above the ambient temperature of 17°C. The O_2 in the vault would be consumed in less than 510 a if it were not for the fact that 78% of the initial O_2 inventory is trapped in the buffer and it only slowly diffuses into the backfill. Of the total inventory of O_2, fully 64% is predicted to be consumed by reaction with Fe(II) released by pyrite dissolution, compared with only 27% in the case of biotite.

The dissolution rate of pyrite is so fast that, on the assumption that there is the same inventory of 3.0 mol·dm^{-2} Fe(II) as for the biotite, all of the pyrite will have dissolved within ~150 a. At that time, 0.8% of the dissolved Fe(II) from the pyrite would have reacted with O_2, 0.1% with Cu^{2+} and the remaining 99% will have accumulated in the backfill and EDZ as dissolved Fe(II) and as a precipitated secondary Fe(II) phase. After the same time, only about 0.1% of the biotite will have dissolved, and that would have been completely converted to Fe(III) by reaction with O_2. Not included in this analysis are the effects of acidification caused by the oxidation of pyrite. The acid produced will be neutralized by adsorption on the clay, although it is possible that additional corrosion could occur if the interfacial pH drops below ~pH 1-2. However, the total amount of acid produced, in moles, is equal to the amount of trapped O_2 (~27 mol/container for the in-room disposal vault) and would be far less than the pH-buffering capacity of the buffer material.

4. DISCUSSION

It is clear from the results of the simulations given above that the engineered barriers can provide almost indefinite containment of the nuclear fuel waste and the radionuclides it contains, regardless of the properties of the geosphere. Most of the simulations presented here were performed with a version of the Cu container model in which the layer of rock between the EDZ and a major fracture does not act as a mass-transport barrier. There appears to be no set of credible geosphere conditions, or, for that matter, incredible conditions, that would lead to failure of a copper container by corrosion in a period of less than 10^6 a. The robustness of the engineered barriers is highlighted by the prediction that the current in-room vault design would prevent O_2 from aerated groundwater from reaching the container for a period of 400 000 a, even if the source of aerated

groundwater was located just 10 cm from the backfill. In reality, groundwater [O_2] are expected to be four orders of magnitude lower (< 1 $ng \cdot g^{-1}$) at a depth of 500 m, thus ensuring containment of the waste for periods >> 10^6 a.

The robustness of the engineered barriers is a result of the slow rate of mass transport and the large excess of Fe(II) minerals and other O_2 scavengers in the vault. Because of the low permeability of the buffer and backfill, the vault is effectively sealed from the O_2 in the groundwater. As a consequence, corrosion of the container is only supported by the O_2 initially trapped in the buffer material, or the Cu^{2+} formed by its reaction with Cu(I). The O_2 trapped in the pores of the backfill is consumed by reaction with Fe(II) prior to diffusing to the container surface. Similarly, O_2 diffusing in through the EDZ from the groundwater is consumed before reaching the container surface.

There is a large excess of Fe(II) minerals in the two conceptual vault designs (the borehole emplacement and in-room configurations). Expressed as a fraction of the initially trapped O_2 in the vault, there is a 50-100 fold excess of Fe(II) in both vault designs. This large excess of Fe(II) helps establish deaerated conditions following vault closure and should maintain anoxic conditions in the vault indefinitely. In addition, the presence of Fe(II) species in the vault, either as dissolved Fe(II) or precipitated Fe(II) secondary phases in the pores of the backfill or fractures of the EDZ or as unaltered biotite in either layer, will act as a redox barrier for oxidized radionuclides released from the container.

This combination of slow mass transport and the excess of Fe(II) minerals effectively ensures indefinite containment of the waste. The extent of container corrosion has been shown to be independent of a wide range of geosphere conditions and backfill properties. The maximum wall penetration due to uniform corrosion is predicted to be < 50 μm which, when added to the maximum pit depth of 6 mm after 10^6 a (King 1996), means that 25-mm-thick Cu containers will not fail by corrosion within this time period.

The distance between the vault and the nearest major water-bearing fracture, the exclusion zone, is shown to have no effect on container lifetimes (Table 2). For a groundwater [O_2] of 1 $ng \cdot g^{-1}$ (the maximum expected value in deep Canadian Shield groundwaters, Gascoyne et al. 1996), the predicted depth of uniform corrosion is ~30 μm for exclusion zone thickness between 1 and 50 m. This independence of container lifetimes on exclusion-zone thickness allows some flexibility in the design and location of the disposal vault. Because the rock between the vault and fracture is not required to act as a mass-transport barrier, the vault would not have to be segmented (other than for vault operational reasons) in the event that a major fracture intersected the vault horizon, as assumed in the reference case study for the EIS (AECL 1994). In addition, the requirements for finding a large area of fracture-free rock are lessened if the vault can be excavated almost to the edge of the fractures.

The calculations presented in Section 3.2 demonstrate the degree to which the engineered barriers can compensate for increases in groundwater [O_2]. At the reference vault depth

of 500-1000 m, there is no evidence that the groundwater [O_2] will exceed 1 $ng \cdot g^{-1}$. At this concentration, the groundwater is an insignificant source of oxidant. Only at groundwater [O_2] > 300 $ng \cdot g^{-1}$ does the ingress of O_2 from the groundwater over a 10^5-a period add significantly to that initially trapped in the vault (Table 3). Sustained groundwater [O_2] this high are inconceivable at the proposed vault depth. These analyses also show that the vault will continue to function as designed if aerated water should penetrate to vault depth for a period of time as a result of tectonic or glacial upheaval.

Increasing the permeability of the EDZ for diffusive mass transport has no effect on container corrosion either. Even if the major fracture is assumed to be located at the EDZ/rock boundary, a highly permeable EDZ will not result in a significant increase in the amount of container corrosion. The results of the simulations suggests that, for a groundwater [O_2] of 1 $ng \cdot g^{-1}$, the low permeability and redox buffering capacity of the backfill will prevent additional corrosion over a period of at least 10^5 a.

In the simulations discussed here, the backfill acts as the primary source of redox-active minerals. There appears to be no great advantage in using more finely graded crushed rock for the dense backfill, since the time to consume the initially trapped O_2 in the vault is not greatly reduced (Table 5). The light backfill defined for the in-room disposal concept (a 1:1 mixture of granitic sand and Na-bentonite) does consume O_2 significantly faster than the dense backfill because of the ~11-fold increase in the exposed surface area of biotite. This increase in surface area will approximately compensate for the ~9-fold increase in O_2 content of the light backfill, which results from its lower density (higher overall porosity) and its lower emplacement moisture content (greater fraction of air-filled voids).

The expected temperature increase in the backfill should be an important design criterion for an actual disposal vault. If the heat output of the fuel is significantly less than that of the reference 10-a-cooled fuel assumed in the EIS, the backfill may be substantially cooler than currently predicted. The consequence of cooler backfill is a reduced rate of biotite dissolution, so that it takes longer to consume the O_2 in the vault (Table 5) and less dissolved and precipitated Fe(II) accumulates in the backfill.

The detrimental effects of cooler temperatures could be offset by using a more active O_2-scavenging mineral. For instance, local Lac du Bonnet granite contains up to 1 wt.% Fe_3O_4, whose rate of oxidation is ~100 times faster than biotite (Taylor and Owen 1997). Thus, actual O_2-consumption rates may be higher than predicted here. Alternatively, pyrite could be added to the buffer, since the rate of consumption of O_2 by pyrite is ~1000 times faster than for biotite. As a consequence, not only would the trapped O_2 be consumed faster, but more Fe(II) would accumulate in the vault (Table 5). The rapid accumulation of Fe(II) could be particularly beneficial in retarding the migration of oxidized radionuclides released from defected containers that fail prematurely. For instance, TcO_4^- released from the container might diffuse rapidly through the buffer, but would be retarded in the backfill by the Fe(II)-mediated reduction to sparingly soluble

TcO_2. Consequently, it would be advantageous to add an excess of pyrite to the backfill to retard the migration of TcO_4^- released from rapidly failing containers.

There is far less Fe(II) in the buffer than in the backfill, and the question arises whether a redox additive should be added to the buffer. Per unit volume, buffer contains almost twice as much trapped O_2 as the dense backfill material. From the viewpoint of container corrosion, however, there is clearly no need to add an O_2 scavenger to the buffer. The predicted depth of uniform corrosion is minimal, even for container wall thickness less than the reference thickness of 25 mm. There may be some advantage if the depth of pitting were significantly less in the presence of a redox additive. However, it is believed that the extent of pitting is greatly overestimated for the current vault design and that the true extent of localized attack will be much less than the current conservative estimate of 6 mm (King 1996).

One of the assumptions made for these simulations was that the vault is saturated at all times and that the O_2 initially trapped in the void spaces is immediately dissolved in the pore water in the buffer and backfill materials (Table 1). Whilst the assumption that the backfill is saturated may be reasonable, the buffer closest to the container may become partially desiccated. In that case, the O_2 in the buffer would be consumed in a shorter period as it would diffuse more rapidly to those locations at which it is reacting (either the container surface or the backfill). In addition, the vault would still be effectively sealed against the ingress of O_2 from the groundwater because of the low rates of mass transport in the saturated backfill material. The assumption that the O_2 in the air-filled voidspace immediately dissolves in the pore water results in artificially elevated $[O_2]$ in the vault. As a consequence, the rate of any process that is proportional to the $[O_2]$ increases. Thus, the predicted rates of O_2 diffusion and reaction with Fe(II) or Cu^{2+} are higher than would be expected. This assumption was made, however, to ensure that all the O_2 initially trapped in the buffer and backfill materials is conserved in the model simulations.

A second assumption was that there is no consumption of O_2 in the buffer due to the microbially mediated oxidation of organic matter (Table 1). There is some experimental evidence to suggest that this process may consume significant amounts of O_2 (Kolář and King 1996). Based on the results of preliminary calculations, inclusion of this process could reduce the predicted time to consume the O_2 in the vault by a factor of 10 (Kolář and King 1996). However, little is known about this process, and further study is required before an accurate assessment of the extent of O_2 consumption by organic carbon can be made.

Deep Canadian Shield groundwaters are found to contain measurable quantities of Fe(II) (Gascoyne 1988). This observation is consistent with the belief that deep groundwaters are O_2-free. Nevertheless, the groundwaters were assumed to be free of Fe(II) for the simulations so that any O_2 in the groundwater would only be consumed as a result of Fe(II) dissolving from the backfill or EDZ. Had this assumption not been made, we would have been faced with the contradictory position that the modelled groundwaters contained both Fe(II) and O_2. In addition, increasing the groundwater $[O_2]$, as in

Section 3.2, would have simply resulted in faster consumption at the EDZ/rock interface due to the presence of an (assumed) infinite source of dissolved Fe(II). It should be reasserted, however, that all available geochemical evidence indicates that deep Canadian Shield groundwaters are essentially O_2-free and contain measurable quantities of Fe(II).

The fourth assumption made (Table 1) was that the interfacial reduction of Cu^{2+} was possible, resulting in corrosion of the container. The results of the simulations indicate that the reduction of Cu^{2+} supports the vast majority of the corrosion reaction, since $\int i_{O2}$ amounted to only ~1% of $\int i_{CORR}$ (Tables 2-5). In an actual disposal vault, it is not certain to what extent the reduction of Cu^{2+} would support the corrosion of a Cu container and to what degree the reduction of O_2 would be the major cathodic reaction. Precipitation of an electrically insulating $CuCl_2 \cdot 3Cu(OH)_2$ porous surface film might inhibit Cu^{2+} reduction, whilst allowing O_2 reduction to occur on the surface of an underlying Cu_2O layer (King 1996). Inclusion of Cu^{2+} reduction leads to a conservative estimate of the corrosion rate.

Mass transport in the four layers was assumed to occur by diffusion only. Advection was not included in the model (Table 1). Whilst this is a reasonable assumption for the buffer, some advective mass transport might be possible in the more hydraulically conductive backfill and certainly in the stress-induced EDZ. By definition, diffusion is the major mass-transport mechanism in the sparsely fractured rock layer. The exclusion of advection in the backfill and EDZ may have resulted in an underestimate of the flux of O_2 into and out of the vault. The degree to which this effect would alter the results obtained is not known.

The groundwater $[Cl^-]$ was assumed to be 0.18 $mol \cdot dm^{-3}$ with no gravitational mixing of saline rock-mass fluids (Table 1). This is a reasonable assumption since most of the simulations were performed with the centrHnr version of the code, in which rapid groundwater flow is imposed at the EDZ/rock boundary. Under these circumstances, the water-rock interaction times would be too short to allow for the development of saline pore fluids.

Finally, the buffer and backfill layer thickness were scaled so that the total volume of these materials was the same as that for the in-room disposal concept (Table 1). Thus, although the exact dimensions used in the simulations might vary from those in the vault, the quantity of trapped O_2 is the same.

The impact of the choice of model and control parameters should also be considered. As previously stated, most of the simulations were run using the centrHnr version of the code. With this model, there is no effect of the sparsely fractured rock on the mass transport of species to and from the vault. The concentration of the various solutes is either maintained constant at this boundary (in the case of O_2 and Cl^-) or is set to zero (in the case of all Cu and Fe(II) species). The effect is that of having fast flowing groundwater separated from the vault by only a thin 10- or 30-cm-thick EDZ. This results in a conservative model for radionuclide transport calculations, but has little effect on the extent of corrosion of the container, which is primarily determined by the quantity

of O_2 trapped in the vault initially. Furthermore, the vault is effectively sealed against O_2 ingress by the low-permeability buffer and backfill and the presence of a significant redox barrier.

In the interests of running a large number of simulations in a short period of time, the control parameters in the model were adjusted to decrease the execution time. As a consequence, the accuracy of the predictions is lower than that obtained from slower runs. At each time interval (of which there would typically be 1000 to 10 000 for a given run), approximately 4000 simultaneous equations are solved, one for each of the 10 chemical species at each of the approximately 400 grid points. In addition, the code calculates the temperature at each grid point at each time interval. An added complexity is that all the rate constants and diffusion coefficients are temperature dependent, so that their values vary spatially and temporally with the temperature gradients in the vault. Because of this complexity, a single, low-accuracy run took several hours to complete. At higher accuracy, each of the 14 runs reported would have taken several days to complete.

The impact of using a lower accuracy was determined by comparing the results of shorter runs of different accuracy. The smaller the interval between time steps, the closer the sum of all the O_2-consumption reactions was to the original quantity of 0.0111 $mol \cdot dm^{-2}$ O_2. However, even in runs of lower accuracy, the sum of the fluxes for the four O_2-consumption reactions, as expressed as a fraction of the initial inventory of O_2, was > 0.93 (Tables 3-5). Consequently, the maximum error associated with those reactions or processes integrated spatially over the three (or four) layers (such as the extent of Cu(I) and Fe(II) oxidation or the amounts of accumulated $Fe(II)_{aq}$ and $Fe(II)_{ppt}$) is estimated to be <10%. Those processes integrated over time (such as $\int i_{O2}$ or $\int i_{CORR}$) are believed to be less accurate, partly because of the larger observed unsystematic variation of $\int i_{CORR}$.

5. SUMMARY AND CONCLUSIONS

The effects of variations in geosphere conditions and of the properties of the backfill material have been examined using a numerical Cu container failure model. The thickness of the exclusion zone between the vault and the nearest major water-bearing fracture has been varied between 1 and 50 m. The groundwater $[O_2]$ has been varied between limits of 1 and 7360 $ng \cdot g^{-1}$, the latter value being equivalent to the hypothetical situation of aerated groundwater. The properties of the excavation-disturbed zone have been varied to simulate both blast-induced and stress-induced damage. Finally, the effects of the particle size of crushed granite, of reduced heat output from the container and the effect of substituting pyrite for biotite on the performance of the backfill material have been determined. The impact of these variations on the corrosion rate, the extent of the four O_2-consumption reactions and the fate of Fe(II) dissolved from the biotite (or pyrite) in the backfill and EDZ has been examined.

The results of the various simulations suggest that the engineered barriers (the container and the buffer and backfill materials) can isolate the fuel almost indefinitely, regardless of

the geosphere conditions. Thus, there is a certain degree of redundancy in the total system, and the combination of engineered and natural barriers represents a system with a high degree of safety. Copper containers are predicted not to fail by corrosion within the analysis period of $\sim 10^5$ a. Indeed, in any of the simulations considered here, the maximum wall penetration due to uniform corrosion is predicted to be <50 μm. The robustness of the engineered barriers is a result of the low rates of mass transport in saturated buffer and backfill materials and because of the presence of an excess of redox-buffering Fe(II) minerals in the backfill.

The robustness of the vault has been determined in a series of simulations in which the groundwater $[O_2]$ was varied between hypothetical limits of 1 and 7360 $ng \cdot g^{-1}$. Even in the presence of aerated water ($[O_2]$ = 7360 $ng \cdot g^{-1}$) at the EDZ/rock boundary, the vault is predicted to prevent O_2 reaching the container for ~400 000 a. The expected groundwater $[O_2]$ is estimated to be < 1 $ng \cdot g^{-1}$.

The presence, or absence, of a layer of sparsely fractured rock between the vault and the nearest major fracture is not expected to affect the lifetime of the containers. Neither is the presence of blast- or stress-induced excavation damage predicted to impact the performance of the vault.

There may be some advantage to adding, or substituting, pyrite to the backfill material. The faster alteration kinetics of pyrite, when compared with biotite, will result in faster O_2 consumption and could compensate for reduced vault temperatures in the event that the fuel to be disposed of is older than the reference 10-a-cooled fuel assumed for the reference calculations. In addition, the more rapid accumulation of dissolved, but unreacted, Fe(II) in the case of pyrite would act as a redox barrier to the migration of oxidized radionuclides (such as TcO_4^-) from prematurely failed containers. The slower dissolution kinetics of biotite mean that no excess Fe(II) is predicted to accumulate in the vault until 900 a after vault closure. However, the possible detrimental effects of acidification resulting from pyrite oxidation have not been assessed.

ACKNOWLEDGEMENT

The Canadian Nuclear Fuel Waste Management Program is jointly funded by AECL and Ontario Hydro via the CANDU® Owners Group.

REFERENCES

AECL (Atomic Energy of Canada Limited). 1994. Environmental impact statement on the concept for the disposal of Canada's nuclear fuel waste. Atomic Energy of Canada Limited Report, AECL-10711, COG-93-1.

Battino, R., T.R. Rettich and T. Tominaga. 1983. The solubility of oxygen and ozone in liquids. J. Phys. Chem. Ref. Data 12, 163-178.

Baumgartner, P., D.M. Bilinsky, C. Onofrei, Y. Ates, F. Bilsky, J.L. Crosthwaite and G.W. Kuzyk. 1995. An in-room emplacement method for a used-fuel disposal facility - Preliminary design considerations. Atomic Energy of Canada Limited Technical Record, TR-665, COG-94-533.*

Chandler, N.A., E.T. Kozak and C.D. Martin. 1996. Connected pathways in the EDZ and the potential for flow along tunnels. In Proc. EDZ Workshop, "Designing the Excavation-Disturbed Zone for a Nuclear Repository in Hard Rock," J. Martino and C.D. Martin (eds.), Canadian Nuclear Society (Toronto, ON), 25-34.

Frape, S.K., P. Fritz and R.H. McNutt. 1984. Water-rock interaction and chemistry of groundwaters from the Canadian Shield. Geochim. Cosmochim. Acta 48, 1617-1627.

Gascoyne, M. 1988. Reference groundwater composition for a depth of 500 m in the Whiteshell Research Area - Comparison with synthetic groundwater WN-1. Atomic Energy of Canada Limited Technical Record, TR-463.*

Gascoyne, M., J.D. Ross and R.L. Watson. 1996. Hydrogeochemical and geochemical data for the alternative assessment case study for nuclear fuel waste disposal in Canada. Atomic Energy of Canada Limited Technical Record, TR-720, COG-95-543.*

Johnson, L.H., D.M. LeNeveu, F. King, D.W. Shoesmith, M. Kolář, D.W. Oscarson, S. Sunder, C. Onofrei and J.L. Crosthwaite. 1996. The disposal of Canada's nuclear fuel waste: A study of postclosure safety of in-room emplacement of used CANDU fuel in copper containers in permeable plutonic rock: Volume 2: Vault model. Atomic Energy of Canada Limited Report, AECL-11494-2, COG-96-552-2.

King, F. 1996. A copper container corrosion model for the in-room emplacement of used CANDU fuel. Atomic Energy of Canada Limited Report, AECL-11552, COG-96-105.

King, F. and M. Kolář. 1995. Prediction of the lifetimes of copper nuclear waste containers under restrictive mass-transport and evolving redox conditions. CORROSION/95, NACE International, Houston, TX, Paper No. 425.

King, F. and M. Kolář. 1996. A numerical model for the corrosion of copper nuclear fuel waste containers. Mats. Res. Soc. Symp. Proc. 412, Materials Research Society, Pittsburgh, PA, 555-562.

King, F., M. Kolář and D.W. Shoesmith. 1996. Modelling the effects of porous and semi-permeable layers on corrosion processes. CORROSION/96, NACE International, Houston, TX, Paper No. 380. (Also published as Atomic Energy of Canada Limited Report, AECL-11592, COG-96-273).

Kolář, M. and F. King. 1996. Modelling the consumption of oxygen by container corrosion and reaction with Fe(II). Mats. Res. Soc. Symp. Proc. 412, Materials Research Society, Pittsburgh, PA, 547-554.

Kolář, M. and F. King. 1997. A model for the corrosion of copper containers in a Canadian nuclear fuel waste disposal vault. Part 2. The mathematical model, results and discussion. Atomic Energy of Canada Limited Report, AECL-11473, COG-95-521.

Malmstrom, M., S. Banwart, L. Duro, P. Wersin and J. Bruno. 1995. Biotite and chlorite weathering at 25°C. Swedish Nuclear Fuel and Waste Management Company Technical Report, SKB-TR-95-01.

Shoesmith, D.W., B.M. Ikeda and F. King. 1995. An assessment of the feasibility of indefinite containment of Canadian nuclear fuel waste. Atomic Energy of Canada Limited Report, AECL-10972, COG-94-534.

Taylor, P. and D.G. Owen. 1995. Reaction of biotite with aerated aqueous solutions: A preliminary report on the effects of temperature, pH and biotite composition. Atomic Energy of Canada Limited Report, RC-1364, COG-95-022-I.

Taylor, P. and D.G. Owen. 1997. Biotite dissolution and oxygen consumption in aqueous media at 100°C. Atomic Energy of Canada Limited Report, AECL-11571, COG-96-157-I.

Werme, L., P. Sellin and N. Kjellbert. 1992. Copper canisters for nuclear high level waste disposal. Corrosion aspects. Swedish Nuclear Fuel and Waste Management Company Technical Report, SKB-TR-92-26.

Wikjord, A.G., P. Baumgartner, L.H. Johnson, F.W. Stanchell, R. Zach and B.W. Goodwin. 1996. The disposal of Canada's nuclear fuel waste: A study of postclosure safety of in-room emplacement of used CANDU fuel in copper containers in permeable plutonic rock: Volume 1: Summary. Atomic Energy of Canada Limited Report, AECL-11494-1, COG-95-552-1.

---

* Internal report available from SDDO, AECL, Chalk River Laboratories, Chalk River, Ontario K0J 1J0.

TABLE 1

ASSUMPTIONS MADE FOR ALL SIMULATIONS

	Assumption
1	The vault is fully saturated at all times and the O_2 originally in the gas phase is immediately dissolved in the pore water.
2	No O_2 is consumed by the microbially mediated oxidation of organic matter. O_2 is only consumed by container corrosion, oxidation of Cu(I) and Fe(II) or by diffusion out of the vault.
3	There is no Fe(II) present in the groundwater or initially in the buffer, backfill, EDZ or rock layers.
4	The interfacial reduction of Cu^{2+} is assumed to occur, resulting in corrosion of the container.
5	There is no advective mass transport in any of the layers.
6	There is no gravitational mixing due to density differences between saline rock-mass fluids and pore-water fluids in the vault. The $[Cl^-]$ in the four layers is assumed to be a constant value of 0.18 $mol \cdot dm^{-3}$.
7	The thicknesses of the buffer and backfill layers are appropriate for the in-room disposal configuration (Johnson et al. 1996).

TABLE 2

EFFECT OF EXCLUSION-ZONE THICKNESS ON CORROSION OF COPPER CONTAINERS[a]

Exclusion-zone thickness (m)	$\int i_{CORR}$ ($C \cdot dm^{-2}$)[b]	T_{max} (°C)[c]	Time of max. temp. (a)[c]	$\int i_{O2}$ ($C \cdot dm^{-2}$)[d]	O_2 flux out of vault ($mol \cdot dm^{-2}$)[e]	Cu(I) oxidn. ($mol \cdot dm^{-2}$)[f]	Fe(II) oxidn. ($mol \cdot dm^{-2}$)[g]	Accum. $Fe(II)_{aq}$ ($mol \cdot dm^{-2}$)[h]	Accum. $Fe(II)_{ppt}$ ($mol \cdot dm^{-2}$)[h]
1	3830	62.4	9.3	44.0	2.3×10^{-4}	8.1×10^{-3}	1.4×10^{-3}	0.012	0.12
5	3800	66.9	11.1	42.0	6.9×10^{-5}	8.9×10^{-3}	1.6×10^{-3}	0.013	0.13
10	3950	71.3	13.4	45.2	7.6×10^{-5}	7.7×10^{-3}	1.8×10^{-3}	0.014	0.14
50[i]	3300	81.0	30.6	34.8	1.4×10^{-4}	8.4×10^{-3}	3.5×10^{-3}	0.027	0.27

a data from simulations for a period of 10^5 a, unless otherwise stated.
b total integrated corrosion current density. 1000 $C \cdot dm^{-2}$ is equivalent to a wall penetration of 7.4 μm.
c maximum container-surface temperature and the time at which the maximum temperature is attained.
d integrated current density for the interfacial reduction of O_2.
e integrated diffusive flux of O_2 out of the vault determined at the backfill/EDZ boundary.
f amount of O_2 consumed in the oxidation of $CuCl_2^-$.
g amount of O_2 consumed in the oxidation of $Fe(II)_{aq}$.
h accumulated $Fe(II)_{aq}$ and $Fe(II)_{ppt}$ in backfill, EDZ and rock layers.
i simulation for 96217 a.

TABLE 3

EFFECT OF GROUNDWATER OXYGEN CONCENTRATION ON THE PERFORMANCE OF THE VAULT[a]

$[O_2]$ ($ng \cdot g^{-1}$)	$\int i_{CORR}$ ($C \cdot dm^{-2}$)[b]	$\int i_{O2}$ ($C \cdot dm^{-2}$)[c]	O_2 flux out of vault ($mol \cdot dm^{-2}$)[d]	Cu(I) oxidn. ($mol \cdot dm^{-2}$)[e]	Fe(II) oxidn. ($mol \cdot dm^{-2}$)[f]	Fraction of original O_2[g]	Accumulated $Fe(II)_{aq}$ ($mol \cdot dm^{-2}$)[h]	Accumulated $Fe(II)_{ppt}$ ($mol \cdot dm^{-2}$)[h]
1[i]	4250	30.1	8.3×10^{-4}	6.3×10^{-3}	3.0×10^{-3}	0.93	1.7×10^{-2}	0.16
5[i]	4650	28.7	8.3×10^{-4}	6.7×10^{-3}	3.0×10^{-3}	0.96	1.7×10^{-2}	0.17
10	3430	30.2	8.2×10^{-4}	6.4×10^{-3}	3.0×10^{-3}	0.93	1.8×10^{-2}	0.18
30[i]	5220	30.4	8.3×10^{-4}	6.2×10^{-3}	3.2×10^{-3}	0.93	1.8×10^{-2}	0.18
100	3040	34.4	8.2×10^{-4}	6.3×10^{-3}	3.4×10^{-3}	0.96	1.8×10^{-2}	0.18
300	3240	35.7	8.1×10^{-4}	7.6×10^{-3}	4.3×10^{-3}	1.2	1.8×10^{-2}	0.18
1000[i]	3320	30.4	8.0×10^{-4}	7.4×10^{-3}	7.5×10^{-3}	1.4	1.7×10^{-2}	0.17
3000[i]	4700	30.1	7.5×10^{-4}	9.9×10^{-3}	1.2×10^{-2}	2.0	1.5×10^{-2}	0.15
7360	3710	36.0	6.1×10^{-4}	2.9×10^{-2}	2.5×10^{-2}	4.9	1.3×10^{-2}	0.13

[a] data from simulations for a period of 10^5 a, unless otherwise stated.

[b] total integrated corrosion current density. 1000 $C \cdot dm^{-2}$ is equivalent to a wall penetration of 7.4 μm.

[c] integrated current density for the interfacial reduction of O_2.

[d] integrated diffusive flux of O_2 out of the vault determined at the backfill/EDZ boundary.

[e] amount of O_2 consumed in the oxidation of $CuCl_2^-$.

[f] amount of O_2 consumed in the oxidation of $Fe(II)_{aq}$.

[g] sum of $\int i_{O2}$, the integrated flux of O_2 out of vault, and the amounts of O_2 consumed by reaction with $CuCl_2^-$ and Fe(II), expressed as a fraction of the amount of O_2 trapped initially in the buffer and backfill materials.

[h] accumulated $Fe(II)_{aq}$ and $Fe(II)_{ppt}$ in backfill and EDZ layers.

[i] simulations for 73521 a, 78325 a, 92746 a, 97551 a and 73515 a for $[O_2]$ of 1, 5, 30, 1000 and 3000 $ng \cdot g^{-1}$, respectively.

TABLE 4

EFFECT OF EXCAVATION-DISTURBED ZONE PROPERTIES ON CORROSION OF COPPER CONTAINERS[a]

k_M $(m \cdot s^{-1})^b$	$\int i_{CORR}$ $(C \cdot dm^{-2})^c$	$\int i_{O2}$ $(C \cdot dm^{-2})^d$	O_2 flux out of vault $(mol \cdot dm^{-2})^e$	Cu(I) oxidn. $(mol \cdot dm^{-2})^f$	Fe(II) oxidn. $(mol \cdot dm^{-2})^g$	Accum. $Fe(II)_{aq}$ $(mol \cdot dm^{-2})^h$	Accum. $Fe(II)_{ppt}$ $(mol \cdot dm^{-2})^h$	Fraction of original O_2[i]	Time for O_2 consumption (a)[j]
5×10^{-12}	4250	30.1	8.3×10^{-4}	6.3×10^{-3}	3.0×10^{-3}	0.017	0.17	0.93	1670
2×10^{-9}	6220	26.5	1.6×10^{-3}	5.7×10^{-3}	5.2×10^{-3}	0.012	0.12	1.1	1400

a data from simulations for a period of 73510 a.

b k_M is the steady-state diffusive mass-transfer coefficient defined by Equation (2) in the text. A value of 5×10^{-12} $m \cdot s^{-1}$ is representative of blast-induced damage and a value of 2×10^{-9} $m \cdot s^{-1}$ represents a stress-induced EDZ.

c total integrated corrosion current density. 1000 $C \cdot dm^{-2}$ is equivalent to a wall penetration of 7.4 μm.

d integrated current density for the interfacial reduction of O_2.

e integrated diffusive flux of O_2 out of the vault determined at the backfill/EDZ boundary.

f amount of O_2 consumed in the oxidation of $CuCl_2^-$.

g amount of O_2 consumed in the oxidation of $Fe(II)_{aq}$.

h accumulated $Fe(II)_{aq}$ and $Fe(II)_{ppt}$ in backfill and EDZ layers.

i sum of $\int i_{O2}$, the integrated flux of O_2 out of vault, and the amounts of O_2 consumed by reaction with $CuCl_2^-$ and Fe(II), expressed as a fraction of the amount of O_2 trapped initially in the buffer and backfill materials.

j time to reduce O_2 content of buffer, backfill and EDZ layers to < 0.01% of the original value.

TABLE 5

EFFECT OF BACKFILL PROPERTIES ON CORROSION OF COPPER CONTAINERS AND VAULT PERFORMANCE[a]

	$\int i_{CORR}$ ($C \cdot dm^{-2}$)[b]	$\int i_{O2}$ ($C \cdot dm^{-2}$)[c]	O_2 flux out of vault ($mol \cdot dm^{-2}$)[d]	Cu(I) oxidn. ($mol \cdot dm^{-2}$)[e]	Fe(II) oxidn. ($mol \cdot dm^{-2}$)[f]	Accum. $Fe(II)_{aq}$ ($mol \cdot dm^{-2}$)[g]	Accum. $Fe(II)_{ppt}$ ($mol \cdot dm^{-2}$)[g]	Fraction of original O_2[h]	Time for O_2 consumption (a)[i]
Effect of biotite surface area A_F = 7.89 dm^{-1}	4650	28.7	8.3×10^{-4}	6.7×10^{-3}	3.0×10^{-3}	0.017	0.17	0.96	1670
A_F = 15.7 dm^{-1}	2700	30.0	4.9×10^{-4}	6.1×10^{-3}	4.2×10^{-3}	0.034	0.33	0.97	1330
A_F = 88.5 dm^{-1}	3670[j]	24.2	6.3×10^{-5}	5.3×10^{-3}	6.0×10^{-3}	0.18	1.8	1.02	860
Effect of temperature H_0 = 0.42 $W \cdot dm^{-2}$	4650	28.7	8.3×10^{-4}	6.7×10^{-3}	3.0×10^{-3}	0.017	0.17	0.96	1670
H_0 = 0.21 $W \cdot dm^{-2}$	3220	49.1	1.2×10^{-3}	8.4×10^{-3}	1.8×10^{-3}	0.010	0.10	1.05	2850
Effect of Fe(II) mineral biotite	3020[j]	28.7	8.3×10^{-4}	6.7×10^{-3}	3.0×10^{-3}	0.015	0.15	0.96	1670
pyrite	4090[j]	22.4	3.1×10^{-5}	4.6×10^{-3}	7.2×10^{-3} [k]	0.3[k]	2.7[k]	1.06	510

[a] data from simulations for a period of 78300 a, unless stated otherwise.

[b] total integrated corrosion current density. 1000 $C \cdot dm^{-2}$ is equivalent to a wall penetration of 7.4 μm.

[c] integrated current density for the interfacial reduction of O_2.

[d] integrated diffusive flux of O_2 out of the vault determined at the backfill/EDZ boundary.

[e] amount of O_2 consumed in the oxidation of $CuCl_2^-$.

[f] amount of O_2 consumed in the oxidation of $Fe(II)_{aq}$.

[g] accumulated $Fe(II)_{aq}$ and $Fe(II)_{ppt}$ in backfill and EDZ layers.

[h] sum of $\int i_{O2}$, the integrated flux of O_2 out of vault, and the amounts of O_2 consumed by reaction with $CuCl_2^-$ and Fe(II), expressed as a fraction of the amount of O_2 trapped initially in the buffer and backfill materials.

[i] time to reduce O_2 content of buffer, backfill and EDZ layers to < 0.01% of the original value.

[j] simulation times of 63100, 57400 and 57400 a, respectively.

[k] the total inventory of 3.0 $mol \cdot dm^{-2}$ Fe(II) is predicted to have dissolved after 150 a.

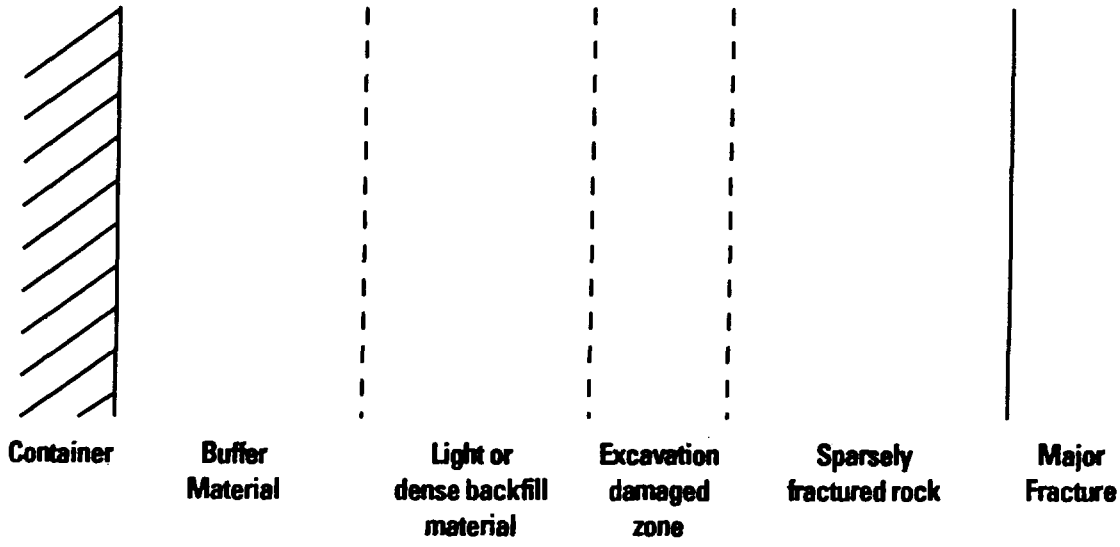

FIGURE 1: Schematic Illustrating the Four Mass-Transport Layers Considered in the Copper Container Failure Model. In the centrH version of the model, the right-hand boundary is located at the sparsely fractured rock/major-fracture interface, whilst for the centrHnr version the boundary is at the EDZ/sparsely fractured rock interface.

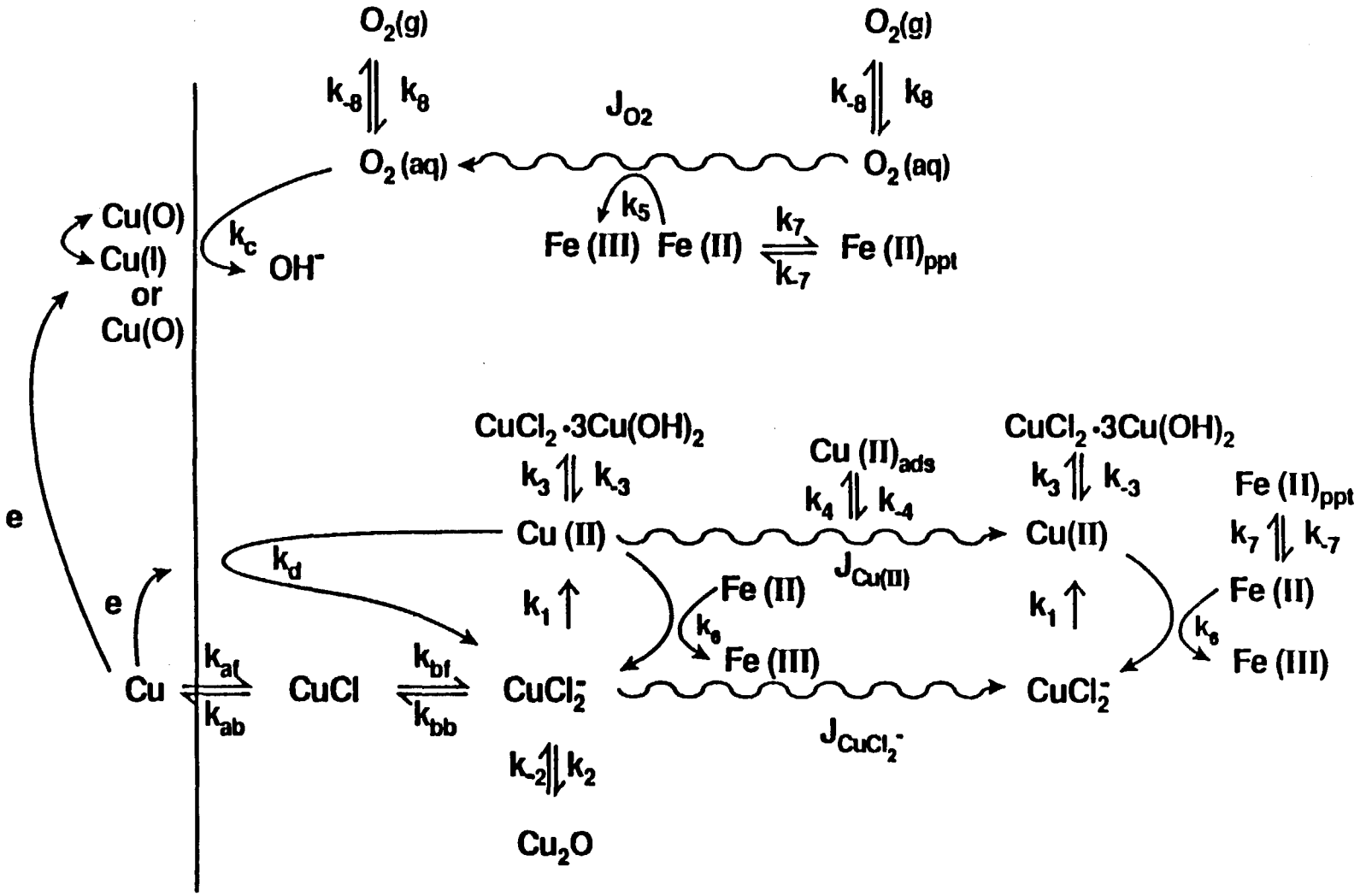

FIGURE 2: The Electrochemical, Chemical and Physical Processes Included in the Copper Container Failure Model

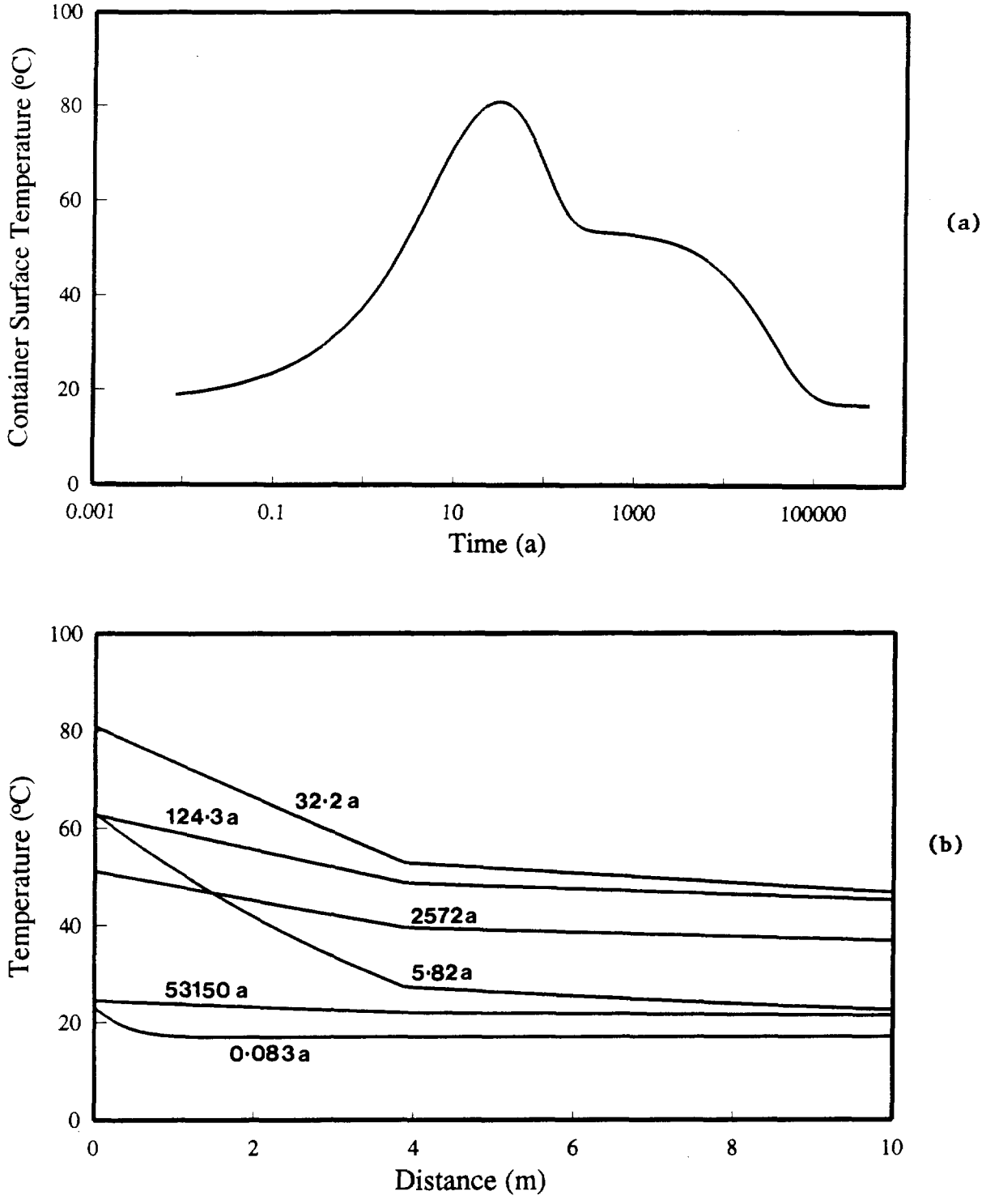

FIGURE 3: Simulated Temperature Profiles for Reference 10-a-Cooled CANDU Fuel. (a) Container surface temperature as a function of time, (b) temperature gradients in the vault for various times (the buffer thickness is 2.4 m and the backfill thickness is 1.47 m. The EDZ is 0.1-m thick).

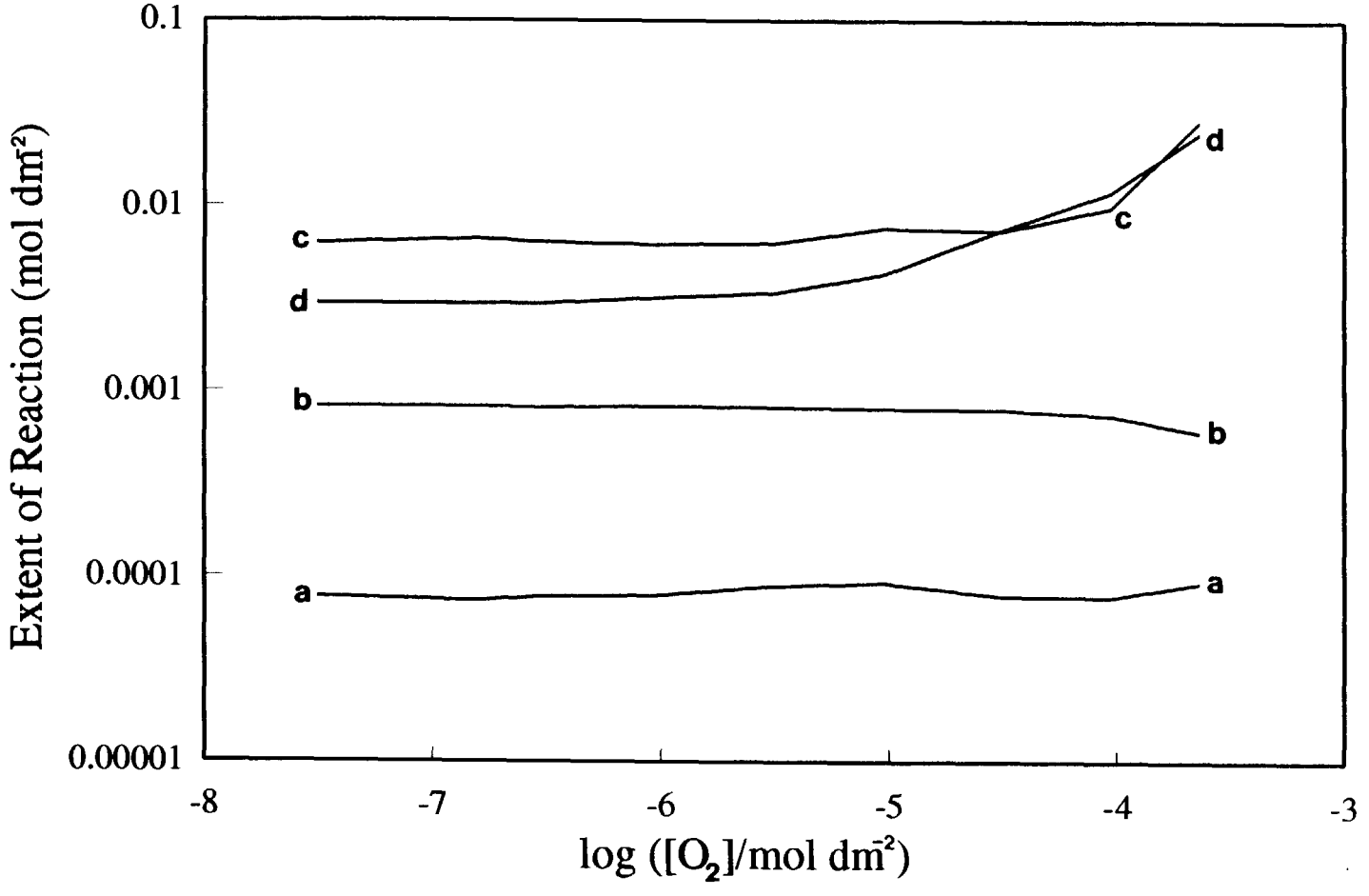

FIGURE 4: The Integrated Reaction Rates for the Four Oxygen Consumption Reactions as a Function of Groundwater $[O_2]$ for a Simulation Period of ~10^5 a. The extent of (a) the interfacial reduction of O_2, (b) the diffusion of O_2 out of the vault, (c) the oxidation of $CuCl_2^-$ by O_2, and (d) the oxidation of Fe(II) by O_2 are integrated over the entire simulation period and, where appropriate, over the buffer, backfill and EDZ layers.

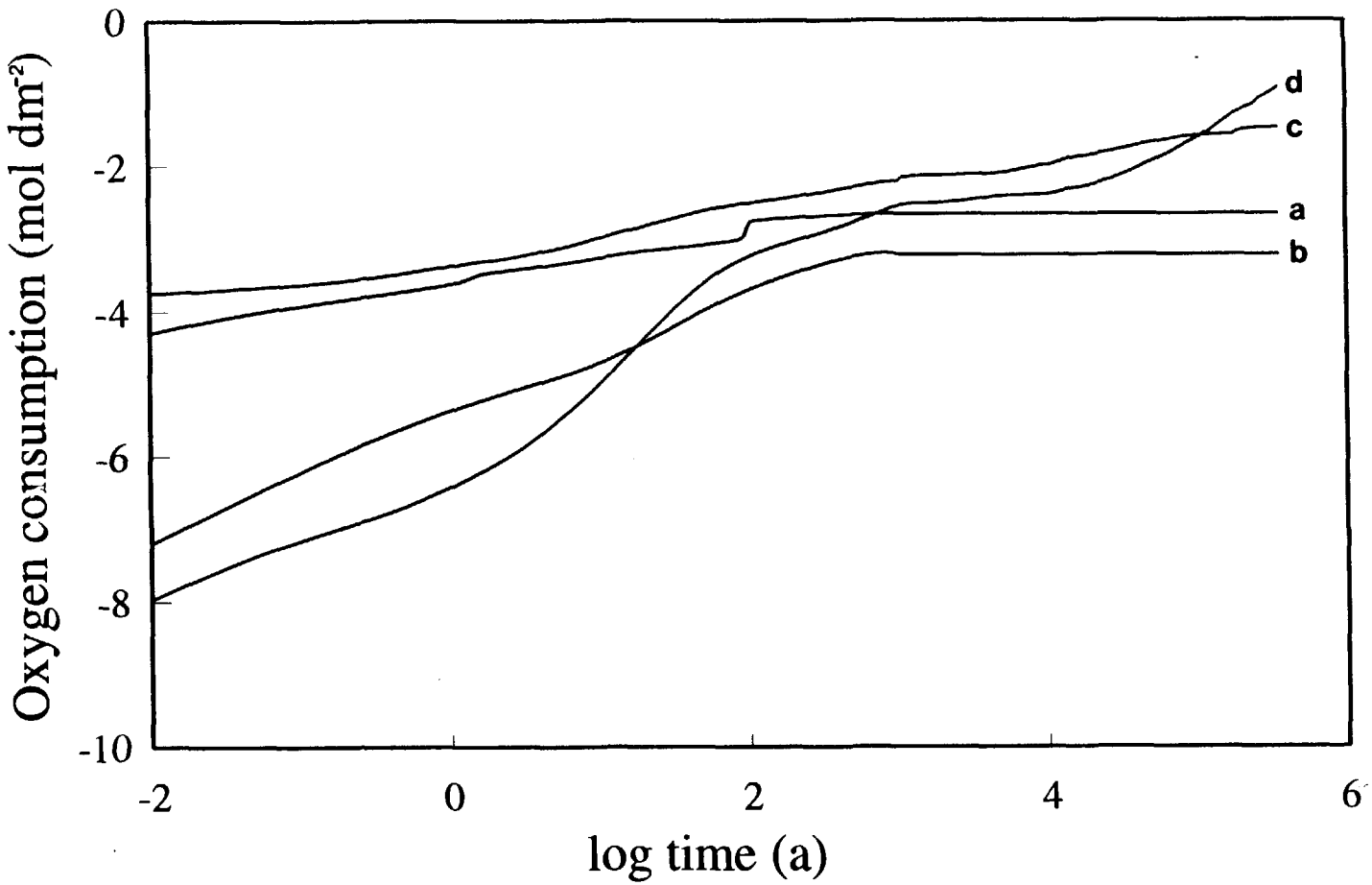

FIGURE 5: The Predicted Time Dependence of the Cumulative Rates of the Four Oxygen Consumption Reactions for a Simulation Period of 3.5×10^5 a in Aerated Groundwater. The extent of (a) the interfacial reduction of O_2, (b) the diffusion of O_2 out of the vault, (c) the oxidation of $CuCl_2^-$ by O_2, and (d) the oxidation of Fe(II) by O_2 are integrated as a function of time and, where appropriate, over the buffer, backfill and EDZ layers.

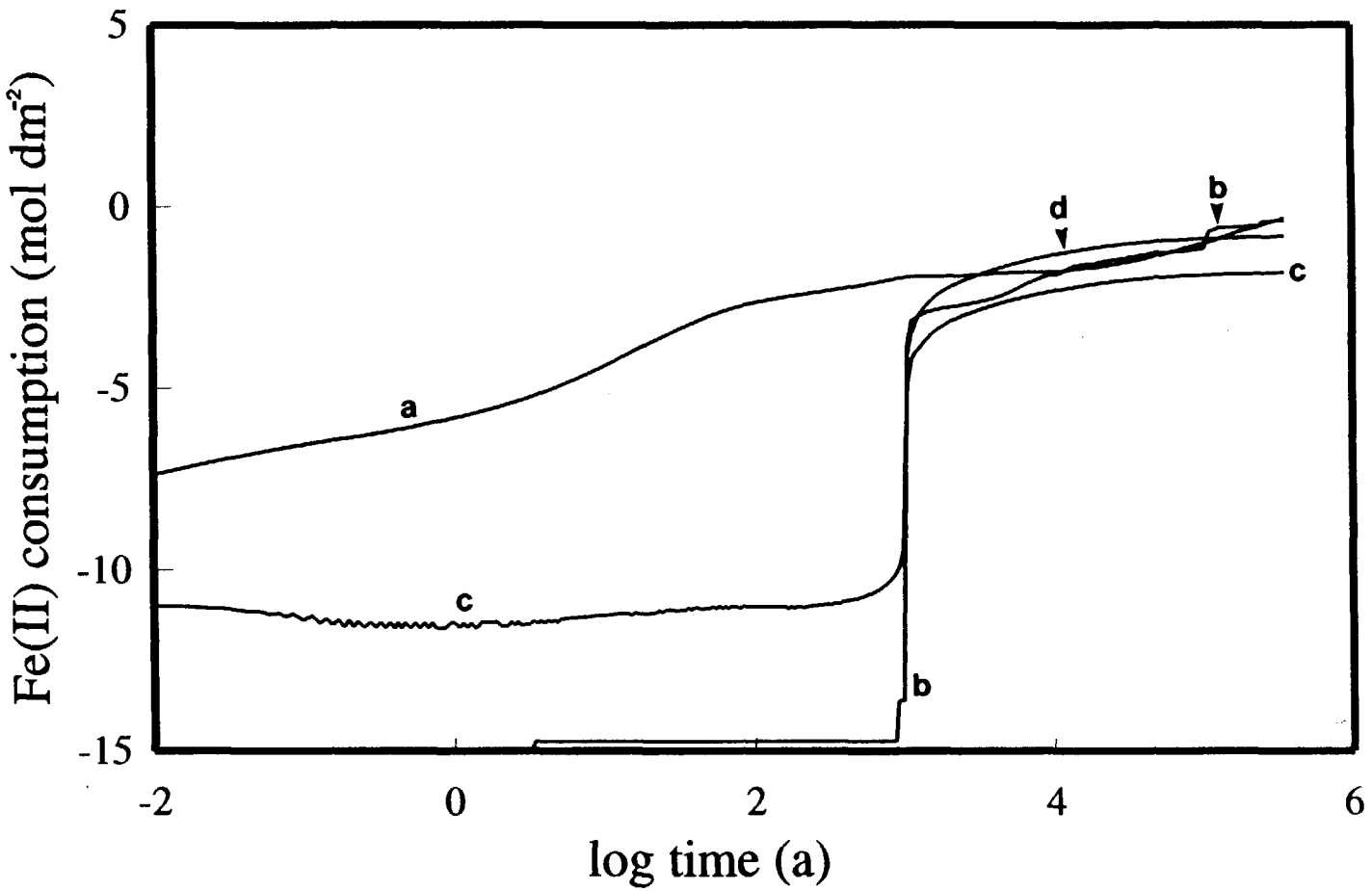

FIGURE 6: The Predicted Time Dependence of the Cumulative Rates of the Four Processes Involving Fe(II) for a Simulation Period of 3.5 x 10^5 a in Aerated Groundwater. The extent of (a) the consumption of Fe(II) by oxidation with O_2, (b) by oxidation with Cu(II), (c) the accumulation of dissolved $Fe(II)_{aq}$ and (d) the accumulation of precipated $Fe(II)_{ppt}$ are integrated over the buffer, backfill and EDZ layers as a function of time.

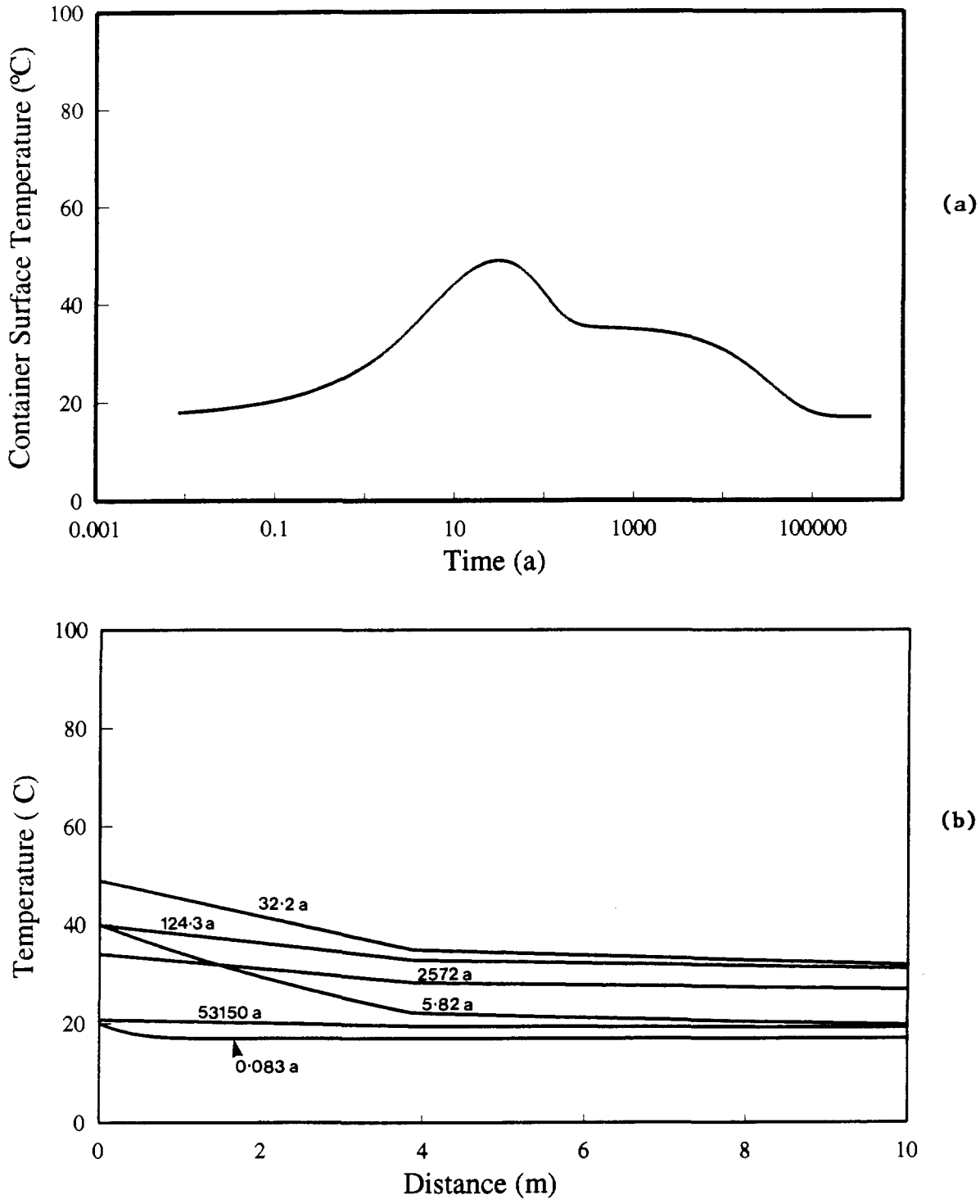

FIGURE 7: Simulated Temperature Profiles for Container with Half the Heat Output as That Shown in Figure 3. (a) Container surface temperature as a function of time, (b) temperature gradients in the vault for various times (the buffer thickness is 2.4 m and the backfill thickness is 1.47 m. The EDZ is 0.1-m thick).

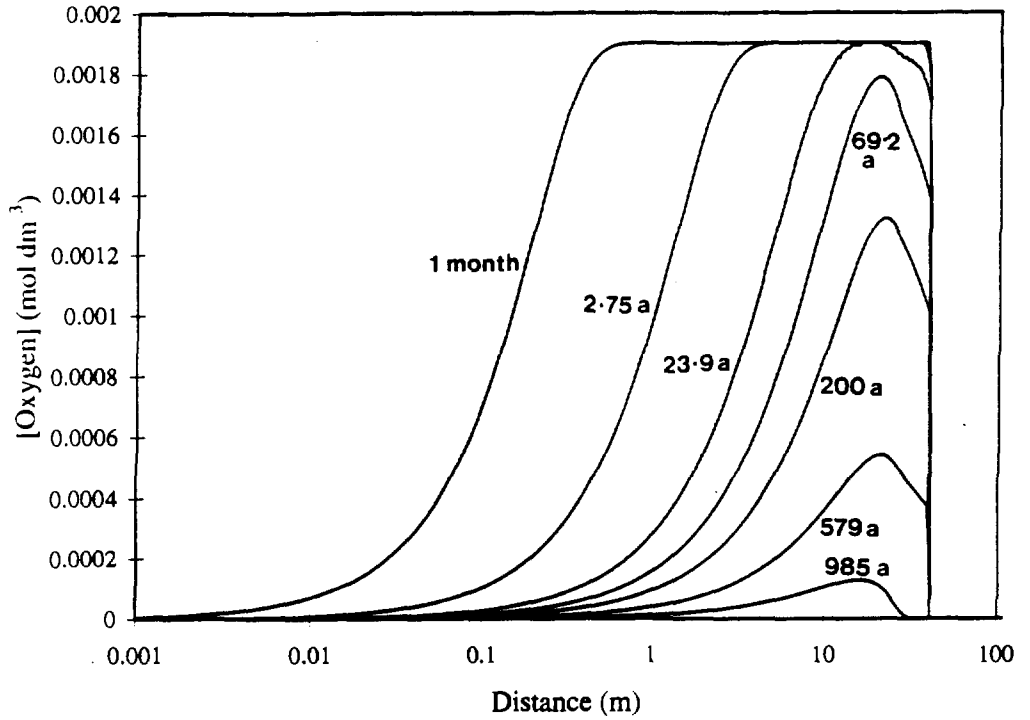

(a)

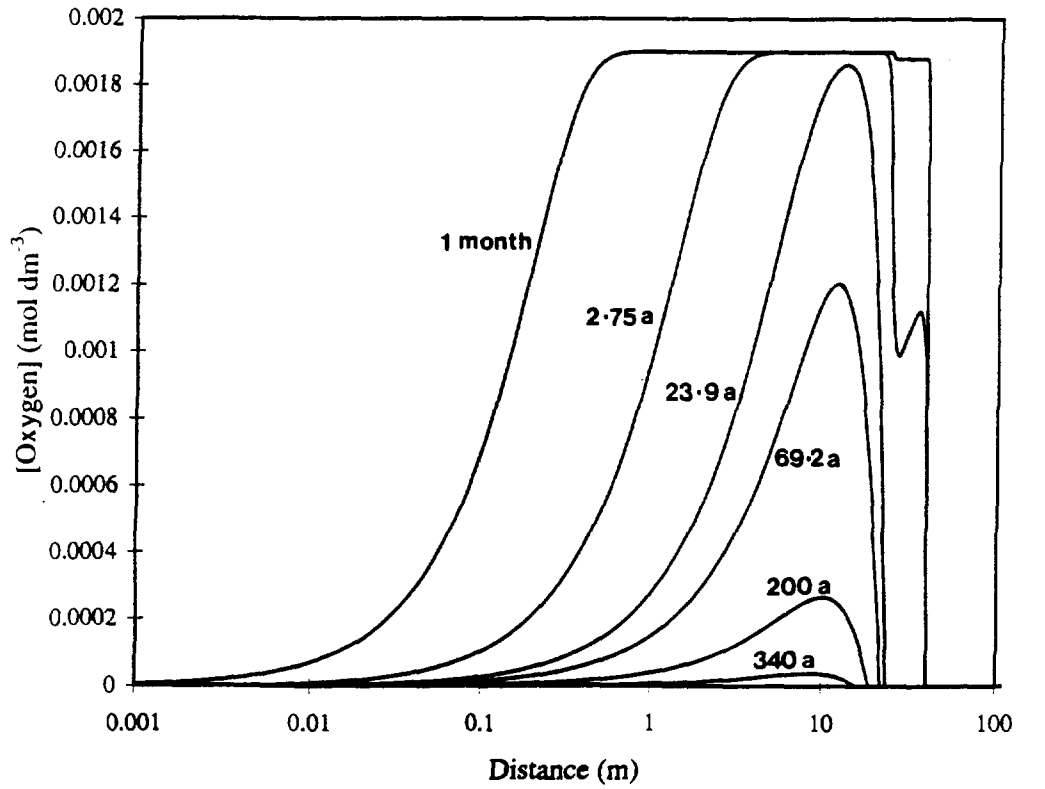

(b)

FIGURE 8: Consumption of Oxygen in the Buffer and Backfill Layers for Different Fe(II)-Containing Minerals. (a) Biotite in backfill, (b) pyrite in backfill (the buffer thickness is 2.4 m and the backfill thickness is 1.47 m. The EDZ is 0.1-m thick).

This page(s) is (are) intentionally left blank.

APPENDIX A

ESTIMATION OF THE SURFACE AREA OF EXPOSED BIOTITE IN BACKFILL MATERIAL

The release rate of Fe(II) from the backfill material depends on the exposed surface area of biotite A_F (Equation (8) of the main text). In the model, A_F is expressed in terms of the surface area per unit volume of backfill and has units of [length]$^{-1}$. The value of A_F depends on the particle size of the crushed granite used to prepare the backfill. Here, A_F will be determined for the reference lower (or dense) backfill defined by Johnson et al. (1994, 1996), for lower backfill containing rock aggregate crushed to a particle size <0.2 cm, and for the upper backfill containing granitic sand, defined for the in-room emplacement study (Johnson et al. 1996).

Consider a collection of spherical particles, of which a mass fraction (f_X) have a diameter (d_X). The surface area and mass of each particle are given by πd_X^2 and $\pi \rho d_X^3/6$, respectively, where ρ is the density of granite (2.65 g·cm^{-3}). The total surface area of all particles per unit mass is, therefore, $\frac{6}{\rho}\sum_X\left(\frac{f_X}{d_X}\right)$. Tables A.1 to A.3 give the assumed particle size distribution and values of (f_X/d_X) for the granite aggregate in the reference lower backfill, for lower backfill containing more-finely crushed rock and for the upper backfill containing granitic sand, respectively.

From Tables A.1 to A.3, the specific surfaces areas for each aggregate are 10.7 cm^2·g^{-1}, 21.3 cm^2·g^{-1}, and 295 cm^2·g^{-1}, respectively. In the reference lower backfill, which has a dry density of 2.1 g·cm^{-3}, the granite comprises 70% of the total mass. Therefore, the surface area of exposed granite in the lower backfill is 15.7 cm^2·cm^{-3}, of which ~5% , or 0.79 cm^2·cm^{-3} (or 789 cm^2·dm^{-3}) is biotite. The corresponding surface area of exposed biotite in the more-finely crushed lower backfill is 1570 cm^2·dm^{-3} and in the upper backfill, which is a 1:1 mixture of clay and granitic sand with a dry density of ~1.2 g·cm^{-3}, 8850 cm^2·dm^{-3}.

TABLE A.1

GRANITE PARTICLE SIZE DISTRIBUTION FOR THE REFERENCE LOWER BACKFILL[a]

d_X (cm)	f_X	f_X/d_X (cm^{-1})
1.59[b]	0.15[b]	0.094
1.14	0.06	0.053
0.74	0.21	0.28
0.36	0.18	0.50
0.18	0.21	1.17
0.09	0.13	1.44
0.05	0.06	1.20
	$\Sigma f_X/d_X$	4.74

[a] Reference lower backfill defined in Johnson et al. (1996)
[b] Particle size distribution taken from Dixon et al. (1994)

TABLE A.2

GRANITE PARTICLE SIZE DISTRIBUTION IN THE LOWER BACKFILL WITH MORE-FINELY CRUSHED ROCK[a]

d_X (cm)	f_X	f_X/d_X (cm^{-1})
0.18	0.53	2.94
0.09	0.33	3.67
0.05	0.14	2.80
	$\Sigma f_X/d_X$	9.41

[a] For the current purposes, the finely crushed backfill material was defined as having a particle size < 2 cm, with d_X values corresponding to the three smallest mesh sizes given by Dixon et al. (1994). The relative mass fractions of these three mesh sizes is the same as that for the reference backfill material.

TABLE A.3

PARTICLE SIZE DISTRIBUTION OF GRANITIC SAND IN THE REFERENCE UPPER BACKFILL[a]

d_X (cm)	f_X	f_X/d_X (cm^{-1})
0.20[b]	0.02[b]	0.10
0.15	0.10	0.67
0.10	0.24	2.40
0.05	0.29	5.80
0.025	0.24	9.60
0.01	0.05	5.00
0.006	0.04	6.67
0.0002	0.02	100.00
	$\Sigma f_X/d_X$	130.2

[a] Reference upper backfill defined in Johnson et al. (1996).

[b] Particle size distribution of granitic sand in the reference upper backfill assumed to be the same as that of silica sand given by Baumgartner et al. (1995).

REFERENCES FOR APPENDIX A

Baumgartner, P., D.M. Bilinsky, C. Onofrei, Y. Ates, F. Bilsky, J.L. Crosthwaite and G.W. Kuzyk. 1995. An in-room emplacement method for a used-fuel disposal facility - Preliminary design considerations. Atomic Energy of Canada Limited Technical Record, TR-665, COG-94-533.*

Dixon, D.A., B.C. Walker, D.S.H. Hnatiw and C. Khole. 1994. Preplacement quality control and as-placed properties of the buffer and backfill materials used in Buffer-Container Experiment 1. Atomic Energy of Canada Limited Technical Record, TR-618, COG-94-36.*

Johnson, L.H., D.M. LeNeveu, F. King, D.W. Shoesmith, M. Kolář, D.W. Oscarson, S. Sunder, C. Onofrei and J.L. Crosthwaite. 1996. The disposal of Canada's nuclear fuel waste: A study of postclosure safety of in-room emplacement of used CANDU fuel in copper containers in permeable plutonic rock. Volume 2: Vault model. Atomic Energy of Canada Limited Report, AECL-11494-2, COG-95-552-2.

---

* Unrestricted, unpublished report available from Scientific Document Distribution Office (SDDO), Atomic Energy of Canada Limited, Chalk River Laboratories, Chalk River, Ontario K0J 1J0.

Cat. No. / Nº de cat.: CC2-11717E
ISBN 0-660-17265-8
ISSN 0067-0367

To identify individual documents in the series, we have assigned an AECL- number to each. Please refer to the AECL- number when requesting additional copies of this document from

Scientific Document Distribution Office (SDDO)
AECL
Chalk River, Ontario
Canada K0J 1J0

Fax: (613) 584-1745 Tel.: (613) 584-3311
ext. 4623

Price: B

Pour identifier les rapports individuels faisant partie de cette série, nous avons affecté un numéro AECL- à chacun d'eux. Veuillez indiquer le numéro AECL- lorsque vous demandez d'autres exemplaires de ce rapport au

Service de Distribution des documents officiels (SDDO)
EACL
Chalk River (Ontario)
Canada K0J 1J0

Fax: (613) 584-1745 Tél.: (613) 584-3311
poste 4623

Prix: B